Low Richardson Number Turbulence in the Ocean Surface Layer

by

Simon Holgate
BSc, University of Liverpool, 1995

A Thesis submitted in Partial Fulfillment of the
Requirements for the Degree of

MASTER OF SCIENCE

in the

SCHOOL OF EARTH AND OCEAN SCIENCES

We accept this thesis as conforming
to the required standard

[redacted]

Dr. R. Lueck, Supervisor (School of Earth and Ocean Sciences)

[redacted]

Dr. R. Chapman, Co-Supervisor (School of Earth and Ocean Sciences)

[redacted]

Dr. R. Stewart, Departmental Member (School of Earth and Ocean Sciences)

[redacted]

Dr. C. Garrett, Outside Member (Department of Physics)

[redacted]

Dr. R. Dewey, External Examiner (Centre for Earth and Ocean Research,
University of Victoria)

Supervisor: Dr. R. Lueck

Abstract

The ocean surface layer is the interface through which most of the transfers of heat and momentum which drive the ocean and atmosphere must pass. Parameterization of turbulent mixing in the ocean is necessary in order to account for these small scale processes which cannot be explicitly treated in large scale models. For parameterizations to be useful, the physics of the processes, and the contexts in which they are valid, must be clearly understood.

Observations of turbulent kinetic energy dissipation, temperature and salinity were made with the instrument *TOMI*, during the Marine Boundary Layer Experiment, which was carried out in Monterey Bay, California, from April 10 to May 5, 1995. Additional data were obtained from a ship mounted Acoustic Doppler Current Profiler, CTD casts, navigational and meterological instruments.

Measurements of a key indicator of mixing, the gradient Richardson number, Ri_g, were found to be below the critical value for instability in a high

shear region of the ocean surface layer, which was maintained close to thermal wind balance. Dissipation levels were high in this low Richardson number region. Despite the evidence for shear instability, temperature gradient skewnesses were not found to follow the expected sign convention, but the distribution of dissipation estimates in the highly turbulent region matched theoretical expectations of lognormality over length scales much greater than those of individual mixing patches. Values of Ri_g measured in highly stratified waters were much greater than the critical value and the distribution of dissipation estimates was found to deviate systematically from lognormal as stratification increased. Dissipation distributions from individual patches continued to conform to the lognormal distribution however.

Comparison was made between direct measurements of the flux Richardson number, Rf, and theoretical/laboratory based estimates. It is shown that theory and laboratory measurements are consistent with a peaking of the flux Richardson number at the point of transition between turbulence and wave-like motions caused by suppression by the stratification, but they are inconsistent with direct measurements of large values of Rf in the highly turbulent region which had a large separation between the energy containing and the dissipative scales. It is conjectured that the process which leads to these large values of Rf has very different physics

from the suppression mechanism and is related to the 2-dimensionality of the energy containing scales in stratified shear flow.

Examiners:

[redacted]

Dr. R. Lueck, Supervisor (School of Earth and Ocean Sciences)

[redacted]

Dr. R. Chapman, Co-Supervisor (School of Earth and Ocean Sciences)

[redacted]

Dr. R. Stewart, Departmental Member (School of Earth and Ocean Sciences)

[redacted]

Dr. C. Garrett, Outside Member (Department of Physics)

[redacted]

Dr. R. Dewey, External Examiner (Centre for Earth and Ocean Research, University of Victoria)

Table of Contents

List of Tables

List of Figures

Acknowledgments

I'd like to thank my supervisor, Rolf Lueck, for giving me the opportunity to work with him in the Ocean Turbulence Laboratory and for providing generous guidance and financial support for my studies. None of this would have been possible without him.

Colleagues, past and present, have been a valuable source of inspiration and motivation. Youyu Lu, Xilong Song and Tian Han have all been there for useful conversation and distraction. Fabian Wolk deserves a special mention as it was from he that I learned much about the workings of *TOMI* over afternoon tea. Fabian also contributed figure 3.1 and the thesis style files. Thanks Fab.

Most of all, I'd like to thank my friends and family for supporting me through both the successes and the failures of the past 3 years.

To my parents and sisters:

More than you ever wanted to know about turbulence ...

For Graham.

Chapter 1

Introduction

Understanding the complex processes of heat, mass and momentum exchange between the atmosphere and the ocean is a huge challenge for oceanographers. Describing these processes in terms of a few easily calculable parameters is the goal of investigators seeking to incorporate sub-grid scale processes into climate models.

The difficulty of parameterization is extremely apparent to oceanographers making measurements at sea. Variability in the ocean means that it is impossible to gain a perfectly synoptic view of the environmental framework within which to interpret the results. Nonetheless, the vast natural laboratory of the sea has significant advantages over the much more controllable environment of the laboratory water channel. In particular, far greater energies are often involved, which leads to a separation between the energy containing scales and the scales of viscous dissipation. This allows the physics of different processes, acting at different scales, to be examined more easily.

The focus of this dissertation will be the dynamics of turbulence generated in a narrow density front, of the order of a few hundred metres wide, and the effects of stratification in suppressing turbulence. Spatial variability in wind mixing and convection can cause horizontal gradients in the density of surface waters, as can

eddies generated by strong currents. This horizontal density variation has an associated horizontal pressure gradient and, as the surface waters re-stratify in response to the gradient, shear is generated between the layers. This shear can generate intense turbulence and mixing.

Shear is considered to become unstable and lead to mixing when a critical gradient Richardson number, $Ri_g = N^2/S^2$ (where N is the buoyancy frequency and S is the shear), is reached. This follows the work of Miles (1961) who showed that $Ri_g < 0.25$ is the critical condition for the onset of turbulence, provided that there is also an inflexion in the velocity profile. Although there is a critical value for the onset of turbulence, once begun, turbulence may be sustained at gradient Richardson numbers larger than 0.25. Laboratory experiments by Thorpe (1973a) suggested that the final gradient Richardson number at the point of suppression of the turbulence was a constant at $Ri_g = 0.322$. Therefore it might be expected that more intense turbulence and hence higher rates of the dissipation of turbulent kinetic energy, ϵ, occur for Richardson numbers around the critical value of 0.25. Oceanographic measurements of Ri_g are presented here which have a higher resolution than has previously been reported and which appear to support this theory.

The relationship of the intensity of the turbulence to the strength of the shear is complicated by the level of stratification resisting the overturning. The amount of kinetic energy which goes into doing work on the stratification and mixing scalar

quantities such as density, is called the buoyant production. The fraction of kinetic energy which goes into the buoyant production, relative to the total production of turbulent kinetic energy by the shear, is known as the flux Richardson number, Rf.

On the basis of energy arguments (Stewart 1959; Osborn 1980), theoretical calculations (Ellison 1957; Townsend 1958), and laboratory experiments (Itsweire *et al.* 1986; Stillinger *et al.* 1983), the flux Richardson number has been suggested to have a maximum value of approximately 0.2. Direct measurements of the buoyancy flux in the ocean are difficult due to the contamination of measured signals by motions of the instrumental platform (Fleury and Lueck 1994). However, some of the direct measurements that do exist (Wolk 1997; Gargett and Moum 1995; Fleury and Lueck 1994) suggest that flux Richardson numbers larger than 0.2 may occur in the ocean. This thesis will attempt to address this problem and will compare oceanographic and laboratory measurements in order to suggest the cause of the difference.

The aim of this thesis then, is to investigate the parameterization of mixing in the ocean surface layer and to examine evidence for the processes which these parameterizations seek to describe. I will concentrate on the following areas:

1. The generation of shear by frontal dynamics.

2. Evidence for the process involved in the dissipation of shear layers.

3. Statistics of the TKE dissipation under different oceanic regimes.

4. The influence of stratification on the flux Richardson number and comparison with laboratory results.

5. Applicability of "similarity scaling" to the ocean surface layer observations.

6. Sampling strategies for complex, evolving environments.

Here, data collected during the second west coast air-sea and meteorology experiment of the Marine Boundary Layer Experiment (MBL II) (Pinkel and Friehe 1996) is presented. MBL II was conducted off the coast of Monterey from April 10 - May 5, 1995 (Julian Days [i.e. days since January 1 1995], JD100-125). Data collected in different shear and stratification regimes by the Towed Ocean Microstructure Instrument (*TOMI*) are explored.

Towed measurements allow good continuous horizontal and temporal coverage of high frequency shear which is not available to vertical profilers. It has long been recognized that mixing occurs in thin layers which are 2-10 m thick (Toole and Schmitt 1987; Gregg 1987) but may extend for several hundred metres horizontally (Gregg *et al.* 1986), giving an aspect ratio of order 1/100 (Rosenblum and Marmorino 1990). Towed vehicles can thus provide a rather different picture of oceanic turbulence than vertical profilers and allow improved statistical significance for results (Wolk 1997).

Chapter 2 sets out the theoretical framework for the thesis. Chapter 3 provides a description of *TOMI* and the other instrumentation and the background oceanographic and meteorological conditions are presented in chapter 4. Chapter 5 covers

the data processing techniques and in chapter 6 results are presented which are discussed in chapter 7. A summary and suggestions for further work conclude the thesis in chapter 8.

Chapter 2

Theoretical Framework

In this chapter the theoretical background to the study of mixing is reviewed and placed in context for use in later chapters.

2.1 The turbulence equations

Turbulence is very difficult to describe precisely, but Tennekes and Lumley (1972) list some of the characteristics of turbulent flows:

Irregularity Turbulent flows are irregular or random so that statistical rather than deterministic methods must be used.

Diffusivity The spreading of velocity fluctuations through the surrounding fluid, causing rapid mixing and increased rates of heat, momentum and mass transfer is an important feature of all turbulent flows.

Large Reynolds' numbers Turbulent flows always occur at high Reynolds' numbers. Instabilities occur which are related to the interaction of viscous and non-linear inertia terms in the equations of motion.

Three dimensional vorticity fluctuations Rotation, 3-dimensionality and high levels of fluctuating vorticity are characteristic of turbulence.

Dissipation Turbulent flows are always dissipative. Viscous shear stresses act to increase the internal energy of the fluid by reducing the kinetic energy of the turbulence.

The equation that is used to describe the motion of a fluid is the Navier-Stokes equation:

$$\rho_0 \frac{\partial V_i}{\partial t} + \rho_0 V_j \frac{\partial V_i}{\partial x_j} + \frac{\partial P_*}{\partial x_i} = \frac{\partial}{\partial x_j}\left(\mu \frac{\partial V_i}{\partial x_j}\right) + \rho_* g_i \tag{2.1}$$

where the first term on the left is the change of velocity with time, the second term is the change in velocity due to advection and the third term is the force exerted by pressure gradients which are departures from the hydrostatic balance. These terms are balanced on the right by viscous dissipation (friction) and body forces acting on the fluid. It is assumed that the fluid is Boussinesq ($\rho = \rho_0 + \rho_*$, $\rho_* << \rho_0$ and $P = P_0 + P_*$, $P_* << P_0$), which is to say that variations in density, ρ_*, are only important in the vertical (i.e when acting with gravity), and ρ_0 is a reference density. In addition, it is convenient to assume incompressibility of the fluid, i.e.

$$\frac{\partial V_i}{\partial x_i} = 0 \tag{2.2}$$

Whilst these equations describe the motion of the fluid as a whole, it is the turbulent fluctuations which are of interest and not the mean flow. The separation into

mean and turbulent parts is achieved using Reynolds' decomposition technique. The following substitutions are employed:

$$V_j = U_j + u_j \tag{2.3}$$

$$\overline{u_j} = 0 \tag{2.4}$$

$$P_* = \Pi + p \tag{2.5}$$

$$\overline{p} = 0 \tag{2.6}$$

$$\rho_* = \overline{\rho} + \rho' \tag{2.7}$$

$$\overline{\rho'} = 0 \tag{2.8}$$

After substituting these into 2.1, dividing by ρ_0 and averaging, Reynolds' equation is obtained:

$$\frac{\partial U_i}{\partial t} + U_j \frac{\partial U_i}{\partial x_j} + \overline{u_j \frac{\partial u_i}{\partial x_j}} + \frac{1}{\rho_0}\frac{\partial \Pi}{\partial x_i} = \mu \nabla^2 U_i + \frac{\overline{\rho}}{\rho_0} g_i \tag{2.9}$$

On subtracting Reynolds' equation (2.9) from the un-averaged Navier-Stokes equation (2.1) we are left with the fluctuating part of the momentum equation.

$$\frac{\partial u_i}{\partial t} + U_j \frac{\partial u_i}{\partial x_j} + u_j \frac{\partial U_i}{\partial x_j} + u_j \frac{\partial u_i}{\partial x_j} - \overline{u_j \frac{\partial u_i}{\partial x_j}} + \frac{1}{\rho_0}\frac{\partial p}{\partial x_i} = \frac{\rho'}{\rho_0} g_i + \nu \nabla^2 u_i \tag{2.10}$$

However, since the mean of the fluctuations is zero this equation must first be multiplied by u_i to obtain the variance and then it can be averaged to give the energy

equation for fluctuations:

$$\frac{1}{2}\frac{D\overline{u_i^2}}{Dt} + \overline{u_i u_j}\frac{\partial U_i}{\partial x_j} + \frac{1}{2}\frac{\partial \overline{u_i u_i u_j}}{\partial x_j} + \frac{1}{\rho_0}\frac{\partial \overline{p u_i}}{\partial x_i} = \frac{\overline{\rho' u_i}}{\rho_0} g_i + \nu \nabla^2 \left(\frac{\overline{u_i^2}}{2}\right) - \nu \overline{\left(\frac{\partial u_i}{\partial x_j}\right)^2} \tag{2.11}$$

where $\nu = \mu/\rho$ is the kinematic viscosity and $D/Dt = \partial/\partial t + U.\nabla$ is the total derivative. The first term on the left is the rate of change of kinetic energy and the advection of kinetic energy by the mean flow, the second term is the rate of working of the Reynolds' stress against the mean flow, the third term is the advection of kinetic energy by the turbulence and the fourth term is the re-distribution of energy by pressure fluctuations. These terms are balanced on the right by losses to work done on the stratification (or gains in buoyancy forced flow), the very small viscous transport term and the rate of viscous dissipation of kinetic energy, ϵ.

We also need the equation for the Reynolds' stress, so taking the i-component of the fluctuating momentum equation (2.10) and multiply by u_k, take the k-component and multiply by u_i, we then add and average to obtain:

$$\frac{D\overline{u_k u_i}}{Dt} + \overline{u_k u_j}\frac{\partial U_i}{\partial x_j} + \overline{u_i u_j}\frac{\partial U_k}{\partial x_j} + \frac{\partial}{\partial x_j}\overline{u_i u_j u_k} + \frac{1}{\rho_0}\left(\overline{u_k \frac{\partial p}{\partial x_i}} + \overline{u_i \frac{\partial p}{\partial x_k}}\right) = \frac{\overline{\rho' u_k}}{\rho_0} g_i + \nu(\overline{u_k \nabla^2 u_i} + \overline{u_i \nabla^2 u_k}) \tag{2.12}$$

If we now consider homogeneous (i.e. the position in space is irrelevant to the statistical description of the turbulence), isotropic (the statistics of the flow are independent of the orientation of the axes), high Reynolds' *TOMI* (Figure 3.1). number flow (that

is to say, there is a large separation between the energy containing scales and the dissipative scales) which is stationary in time (neither growing nor decaying), then we can write the Reynolds' stress equations as:

$i = 1,\ k = 3$

$$\frac{D\overline{wu}}{Dt} = 0 = -\overline{w^2}\frac{\partial U}{\partial z} - \frac{1}{\rho_0}\left(\overline{w\frac{\partial p}{\partial x}} + \overline{u\frac{\partial p}{\partial z}}\right) - \frac{\partial \overline{uw^2}}{\partial z} + \nu(\overline{w\nabla^2 u} + \overline{u\nabla^2 w}) \quad (2.13)$$

$i = k = 1$

$$\frac{D\overline{u^2}}{Dt} = 0 = -2\overline{uw}\frac{\partial U}{\partial z} - \frac{2}{\rho_0}\overline{u\frac{\partial p}{\partial x}} - \frac{\partial \overline{wu^2}}{\partial z} + 2\nu\overline{u\nabla^2 u} \quad (2.14)$$

$i = k = 2,$

$$\frac{D\overline{v^2}}{Dt} = 0 = -\frac{2}{\rho_0}\overline{v\frac{\partial p}{\partial y}} - \frac{\partial \overline{v^2 w}}{\partial z} + 2\nu\overline{v\nabla^2 v} \quad (2.15)$$

$i = k = 3$

$$\frac{D\overline{w^2}}{Dt} = 0 = -\frac{2}{\rho_0}\overline{w\frac{\partial p}{\partial z}} - \frac{\partial \overline{w^3}}{\partial z} - \frac{\overline{\rho' w}}{\rho_0}g + 2\nu\overline{w\nabla^2 w} \quad (2.16)$$

2.2 Turbulence in a stably stratified fluid

Stewart (1959) used the above equations (2.13-2.16) to describe the flow of kinetic energy from the mean flow into 3 components of the turbulence. As can be seen in 2.14, the Reynolds' stress, $\overline{uw}$, removes energy from the mean shear, $\partial U/\partial z$. This kinetic energy is re-distributed into the 3 components of turbulent velocity by the

pressure term which is seen to be the source term in equations 2.15 and 2.16. This is because

$$\overline{u\frac{\partial p}{\partial x}} = \nabla.(\overline{pu}) - \left(\overline{v\frac{\partial p}{\partial y}} + \overline{w\frac{\partial p}{\partial z}}\right) \tag{2.17}$$

where the divergence term represents re-distribution in space and so averages to zero over the volume of the turbulence (provided that there is no boundary within the volume and that there is no flux across the surface of the averaging volume) whilst the pressure term re-distributes kinetic energy to the other components. The third term on the right of 2.14 is the turbulent re-distribution term which is a divergence so again averages to zero over the volume and hence it is neglected in further discussions.

Losses from the u component of the kinetic energy are from viscous dissipation, the fourth term on the right hand side of equation 2.14. The w component (equation 2.16) also loses energy to viscous dissipation but it is only this component which does work against the stratification and this loss is given by the third term on the right.

In order for production to occur, we require $\overline{uw}$ to be non-zero. From the Reynolds' stress equation (2.13) it can be seen that the production of $\overline{uw}$ arises from the interaction of $\overline{w^2}$ with the mean flow. However, $\overline{w^2}$ only receives its energy through re-distribution by pressure fluctuations (equation 2.16). Hence, the suppression of $\overline{w^2}$ will lead to the suppression of turbulence.

Due to the fact that $\overline{w^2}$ is affected both by viscosity and buoyancy forces and because laboratory evidence suggests that the correlation of pressure fluctuations with

velocity fluctuations is poor (as the tendency towards isotropy appears inefficient), Stewart (1959) argued that the proportion of kinetic energy going into the stratification should be considerably less than the loss to viscous dissipation. That implies that the flux Richardson number

$$Rf = \frac{\frac{\overline{\rho' w}}{\rho_0} g}{\overline{uw}\frac{\partial U}{\partial z}} \tag{2.18}$$

should also be considerably less than one.

The hypothesis that there should be a critical flux Richardson number, Rf_{crit}, corresponding to the point at which the proportion of kinetic energy required to do work against the stratification is too great for the turbulence to overturn, had been made prior to Stewart (1959). The case of a flow moving over a surface with constant stress and a constant heat flux was considered by Ellison (1957). Under these conditions, there is homogeneity in the direction of the flow and inhomogeneity in the direction of the shear. Using length scale arguments, Ellison examined the point at which turbulence was no longer sustained, which was considered to be where the ratio of eddy transport of heat to eddy transport of momentum, K_H/K_M, equals zero. At this point turbulence is suppressed so heat transport may only be carried out by molecular diffusion, whilst momentum transport can continue through wave-like motions. In this limit, Ellison (1957) found that

$$\frac{K_H}{K_M} = \frac{(\overline{u^2} + \overline{v^2} + \overline{w^2})\overline{w^2}\,[1 - Rf(1 + T_{\tau 1}(\overline{u^2} + \overline{v^2} + \overline{w^2})/T_{\tau 2}\overline{w^2})]}{2u_*^4(T_{\tau 2}/T_{\tau 3})(1 - Rf)^2} \tag{2.19}$$

where $T_{\tau 1}$, $T_{\tau 2}$ and $T_{\tau 3}$ are the decay times of $\overline{\rho'^2}$, $\overline{u^2}+\overline{v^2}+\overline{w^2}$ and $\overline{w\rho'}$ respectively and u_* is the friction velocity. Ellison then takes $T_{\tau 1}/T_{\tau 2}=1$ and assumes $(\overline{u^2}+\overline{v^2}+\overline{w^2})/\overline{w^2}=5.5$ as found under neutral conditions in the atmosphere. Since for small, positive values of Rf, the term in square brackets is dominant, Ellison evaluated this for $K_H/K_M=0$ to obtain $Rf=0.15$. These assumptions will be examined later in chapter 7.

Townsend (1958) used similar length scale arguments to Ellison (1957) for the case of a flow unrestrained by fluid boundaries which is assumed to be fully turbulent near the origin of the flow and to move through the transition to wave-like flow downstream. Hence the flow is homogeneous in the direction of shear and inhomogeneous in the direction of flow, as with grid generated turbulence. Townsend's arguments led him to

$$Rf=\frac{1}{2}H\left[1-\left(1-12\frac{L_\theta}{L_\epsilon}\frac{K_H^2}{K_M^2}\frac{Ri_g}{H^2}\right)^{1/2}\right] \tag{2.20}$$

where H is a measure of the ratio of the logarithmic rate of radiative cooling of a fluid element to the mean rate of shear and is equal to 1 in the absence of radiative effects and $Ri_g=N^2/S^2$ is the gradient Richardson number as defined in chapter 1. Using the assumption that for high Reynolds' number flows the ratio of characteristic length scales of temperature fluctuations and turbulence are likely to be approximately equal, i.e. $L_\theta/L_\epsilon=1$, and similarly the eddy coefficients for temperature and momentum are also approximately equal ($K_H/K_M\approx 1$), this sets the limits of $Rf<0.5$ for

$Ri_g < 1/12$. Again, these assumptions will be returned to in chapter 7.

The desire to parameterize mixing in the ocean without the complication of attempting to measure the buoyancy flux led Osborn (1980) to define the eddy coefficient for density, K_ρ, by

$$K_\rho = \frac{g}{\rho_0} \frac{\overline{w\rho'}}{N^2} \tag{2.21}$$

which allows K_ρ to be related to ϵ, N and Rf as

$$K_\rho = \frac{Rf\ \epsilon}{(1 - Rf)N^2} \tag{2.22}$$

Osborn then used $Rf \leq Rf_{crit} = 0.15$ to give

$$K_\rho \leq \frac{0.15\epsilon}{0.85N^2} < 0.2\frac{\epsilon}{N^2} \tag{2.23}$$

and this is the parameterization usually used to calculate K_ρ in the ocean.

2.3 Turbulent scales and parameters

The oceanographic literature is full of scales and parameters which are used to define the state of the flow. The purpose of this section is to introduce the scales that are relevant to this thesis and to clarify the inter-relationships of some of the parameters.

Two length scales of particular interest are the Ozmidov scale and the Kolmogorov scale. The Ozmidov scale (Ozmidov 1965) is defined by:

$$L_O \equiv \left(\frac{\epsilon}{N^3}\right)^{1/2} \tag{2.24}$$

and is the length scale at which the inertial forces of active turbulence equal the buoyancy forces of the local stratification. Hence it is considered to define the largest possible scale of overturning in the fluid. The Kolmogorov scale, on the other hand, is defined by:

$$L_K \equiv \left(\frac{\nu^3}{\epsilon}\right)^{1/4} \tag{2.25}$$

and is the scale at which viscous forces equal the inertial forces of active turbulence. The Kolmogorov scale is considered the smallest scale of turbulent motion. A third length scale which is often invoked is that of the largest scale of active turbulence which actually occurs. This is given by the Ellison scale,

$$L_E \equiv \overline{(\rho'^2)}^{1/2} \left(\frac{\partial \rho}{\partial z}\right)^{-1} \tag{2.26}$$

Stacey *et al.* (1997) re-wrote the Ellison scale in terms of a shear based estimate, $L_E = 3(P_t/S^3)^{1/2}$ where P_t is the shear production of turbulence, $P_t = -\overline{uw}S$, and S is the 10 m averaged shear. Since P_t is difficult to measure directly it will be assumed that $P_t \approx \epsilon$ (true for small values of Rf), recognizing that this is an underestimate.

The ratio of the Ozmidov to Kolmogorov scale gives the buoyancy Reynolds' number,

$$Re_b = \left(\frac{L_O}{L_K}\right)^{4/3} = \frac{\epsilon}{\nu N^2} \tag{2.27}$$

The results of Gargett *et al.* (1984) suggest that buoyancy forces significantly effect the inertial subrange of the vertical component of the turbulent velocity when $Re_b <$

200 (i.e. $L_O/L_K = 53$). The laboratory results of Itsweire *et al.* (1986) found that buoyancy production is suppressed at $Re_b \approx 20$. The parameter, $\gamma_t \equiv (\epsilon/\nu)^{1/2}$ [s^{-1}], is defined as the turbulence rate of strain from which we can see that the Kolmogorov scale can also be given by $L_K = (\nu/\gamma_t)^{1/2}$. The turbulence rate of strain also yields the turbulence time scale, $T_t = \gamma_t^{-1}$.

Ivey and Imberger (1991) used the three length scales defined above to calculate two other parameters. The turbulent Froude number is defined as

$$Fr_t = \left(\frac{L_O}{L_E}\right)^{2/3} = \left(\frac{S^{3/2}}{3N^{3/2}}\right)^{2/3} \tag{2.28}$$

From the definition of the gradient Richardson number, Fr_t can thus be written

$$Fr_t \approx 0.48 Ri_g^{-1/2} \tag{2.29}$$

which shows that $Fr_t = 1$ is approximately the same as $Ri_g = 0.25$. A second parameter arises from the ratio of the Ellison scale to the Kolmogorov scale and is called the turbulent Reynolds' number

$$Re_t = \left(\frac{L_E}{L_K}\right)^{2/3} \tag{2.30}$$

which can also be written $Re_t \approx 4.3\epsilon/\nu S^2$ using the definitions above.

A reference list of symbols, scales and common parameters is included in appendix A.

2.4 The log-normality of the dissipation distribution

The random nature of turbulence means that statistical description of the terms is necessary. Even when the Reynolds' number is very high and there is no obvious change in the nature of the turbulence, intermittency is still strong (Grant *et al.* 1962). In order to parameterize mixing we need some sense of 'average' dissipation since this is used to calculate various quantities of interest such as the vertical eddy diffusivity (Osborn 1980) and length scales such as the Ozmidov scale. This requires knowledge of the probability density function (pdf) of ϵ.

Gurvich and Yaglom (1967) applied Kolmogorov's theory of breakage (Kolmogorov 1941b) to the concept of a cascade of turbulent energy from large to small scales. The theory of breakage shows that locally isotropic turbulence will have a log-normal distribution i.e. the logarithm of the distribution will be Gaussian.

To begin with, consider a volume, Q_0, which has a length scale, l_0, of the order $\mathcal{L}$, where $\mathcal{L}$ is the typical scale of motion of the mean flow. Fluctuations of any non-negative characteristic of the turbulence are given by $\varphi = \varphi(\mathbf{x}, t)$. Within Q_0 there is contained a smaller volume, Q_1, with length scale $l_1 < l_0$. Again, within Q_1 there is a contained a smaller volume, Q_2 but with length scale $l_2 = l_1(l_1/l_0) = l_0(l_1/l_0)^2$. Ever smaller volumes, Q_i, can be selected down to some small domain, Q_N, where fluctuations of φ are negligible.

The mean value of the variable $\varphi(\mathbf{x}, t)$ within the volume Q_i is denoted φ_i and

the random variable φ_i/φ_{i-1} is denoted ξ_i. In the case where φ_{i-1} is a constant and only φ_i is random, φ_0 is the same as the expected value, $\overline{\varphi}$, and the variables φ_i with different j will be mutually independent and identically distributed for all indices j such that $l_{i-1} \ll \mathcal{L}$ and $L_{Ki} \ll l_i$ (where $L_{Ki} = (\nu^3/\epsilon_i)^{1/4}$ is the Kolmogorov microscale corresponding to the mean rate of viscous dissipation, ϵ_i, for the domain Q_i). This means that the average value φ_n within the domain Q_n is given by:

$$\varphi_n = \overline{\varphi} \prod_{i=1}^{n} \xi_i \tag{2.31}$$

and

$$\log \varphi_n = \log \overline{\varphi} + \sum_{i=1}^{n} \log \xi_i \tag{2.32}$$

As pointed out by Yamazaki and Lueck (1990), Gurvich and Yaglom (1967) implicitly assume that $\log \xi_i$ is Gaussian. This requires the condition of identical distribution to be fulfilled which in turn requires that the random variables $\log \xi_i$ be drawn from a single population. This means that if the domain Q_0 contains breakages caused by more than one process, $\log \xi_i$ may not be identically distributed.

Yamazaki and Lueck (1990) showed that apparent non-lognormality in observations of oceanic dissipation rates was due to the lack of adherence to the requirement of mutual independence and identical distribution. Yamazaki and Lueck found that when observations were taken from a single turbulent patch (setting the domain scale, $\mathcal{L}$, strictly as the external length scale of the turbulent layer) and observations were

averaged over a length as small as $3L_K$, distributions of ϵ passed the Kolmogorov-Smirnov test for log-normality at the 5% level. This small scale may not actually be sufficient for strictly mutually independent observations as van Atta and Yeh (1975) found that averaging over $36L_K$ was required for statistical independence.

2.5 Temperature gradient skewness

Some evidence of the nature of the process causing the dissipation may be derived from the gradient Richardson number, since shear driven instabilities should have low Richardson numbers, below $Ri_g = 1$. However, it would be interesting to see whether there is other evidence of the shear instability mechanism.

The local isotropy of high Reynolds' number turbulence proposed by Kolmogorov (1941a) states that the probability laws describing velocity differences between neighbouring points should become invariant to translations in space-time or rotations and reflections of the co-ordinate axes. Under these circumstances, the skewness of the streamwise spatial derivative of the fluctuating vertical velocity component $\mathtt{S}_\mathbf{k}(\partial u_3/\partial x_1)$ and of the temperature gradient $\mathtt{S}_\mathbf{k}(\partial T/\partial x_1)$ should be zero. However, both of these quantities have been found to be significantly non-zero (Gibson *et al.* 1977; Stewart 1969).

A non-zero skewness has been shown to be consistent with the concept of local isotropy if it depends only on the large scale flow (Sreenivasan and Antonia 1977).

The skewness of the temperature gradient in turbulent boundary layers has been suggested to result from the straining of the temperature field by the mean shear (Screenivasan and Tavoularis 1980) into ramp-like turbulent structures. The sign of the skewness of the temperature gradient derivative, measured in the flow direction, sgn $S_k(\partial T/\partial x)$, has been found to be given by sgn $[\hat{\mathbf{x}} \cdot (\nabla \mathbf{T} \times \boldsymbol{\omega})]$ (Gibson *et al.* 1977), where $\hat{\mathbf{x}}$ is a unit vector in the mean flow direction, $\nabla \mathbf{T}$ is a vector in the direction of the mean temperature gradient and $\boldsymbol{\omega}$ is the vorticity of the mean flow in the plane parallel to the boundary.

Observational support for the ramp-like structure of temperature derivatives has been found by Antonia *et al.* (1979) in the atmospheric surface layer, by Thorpe and Hall (1980) in the stable mixing layer of Loch Ness and by Thorpe *et al.* (1991) in both the convective ocean surface layer and the bottom boundary layer. In all cases, the sign of the skewness conformed to the sign convention of Gibson *et al.* (1977).

Thorpe and Hall (1980) associate the temperature ramps with Kelvin-Helmholtz type shear instabilities which have dissipation at a maximum at the front. Marmorino *et al.* (1987) found similar temperature ramps in thermistor data from a near-inertial period wave. The data appeared to show instability and overturning at the leading edge of the ramp.

2.6 Similarity scaling

Energy input to the ocean surface layer is primarily through exchanges of heat and momentum with the atmosphere. For several decades, atmospheric studies (e.g Wyngaard *et al.* 1971) have shown that turbulence in the planetary boundary layer can be successfully parameterized if the layer is controlled vertically by horizontally uniform fluxes at the surface. This parameterization is known as similarity scaling. We have already seen in section 2.2 that a knowledge of the level of viscous dissipation is crucial for parameterizing eddy coefficients. However, due to the difficulty of making oceanic measurements, it is only in the last two decades that workers have begun to apply similarity scaling to the oceanic surface layer.

Similarity scaling uses only four variables to determine the average and turbulent structure within the boundary layer:

- the surface heat flux is $J_q^0 \equiv J_q^{sw} + J_q^{lw} + J_q^e + J_q^s$ [Wm^{-2}] where J_q^{sw} is the shortwave radiative flux, J_q^{lw} is the longwave radiative flux, J_q^e is the evaporative heat flux and J_q^s is the sensible heat flux. By convention, positive fluxes are defined as losses from the ocean to the atmosphere.

- the friction velocity at the surface, $u_* \equiv \sqrt{\tau}/\rho$ [ms^{-1}], where τ is the wind stress in pascals

- the distance from the surface, z [m]

- the buoyancy flux, $J_b^0 \equiv g/\rho(-\alpha J_q^0/c_p + \beta s J_q^e/L_e(1-s)$ [WKg^{-1}], where g is the acceleration due to gravity, α is the coefficient of thermal expansion, c_p is the specific heat of seawater at constant pressure, β is the coefficient of haline contraction, L_e is the latent heat of evaporation and s is the salinity in concentration units.

Only three of these variables are independent, but a fourth can be determined from these three which is known as the Monin-Obukhov length,

$$L \equiv \frac{-u_*^3}{\kappa J_b^0} \tag{2.33}$$

and gives the distance from the surface at which wind stress and buoyancy forces are equally effective at producing turbulence. Here, κ is von Kármán's constant and has the value 0.4. The minus sign means that L is negative when the surface buoyancy flux (loss from the ocean to the atmosphere) is positive. Hence where $z/-L << 1$, wind stress dominates the production of turbulence and when $z/-L >> 1$, buoyancy is the main source of turbulence.

In the surface layer dominated by wind stress, the non-dimensional dissipation is given by (Lombardo and Gregg 1989)

$$\epsilon_s = \frac{u_*^3}{\kappa z} \tag{2.34}$$

whereas in the buoyancy dominated surface layer the scaling is

$$\epsilon_f = J_b^0 \tag{2.35}$$

and below the surface layer, in the mixed layer, away from the direct influence of the wind, ϵ_{ml} is also equal to J_b^0. When non-dimensionalized by the appropriate parameter for the regime, the non-dimensional dissipation, ϵ_*, is simply a function of z/L which has to be determined by experiment.

Anis and Moum (1992) found that near to the surface of the ocean, higher dissipation rates were measured than could be explained by wind stress scaling. Anis and Moum suggested that other processes may contribute to the rate of viscous dissipation in the ocean surface layer, such as wave-induced mean drift increasing effective values of u_*, Langmuir cells causing episodic mixing events or surface waves acting to intensify the turbulence.

Chapter 3

Instrumentation

The operations of this component of the MBL II experiment were conducted from the R/V *Wecoma*. In this chapter the instrumentation used in our data collection is described.

3.1 Microstructure measurements

Central to our experiment is the Towed Ocean Microstructure Instrument, *TOMI* (Figure 3.1). Similar to its predecessor, *HOTDAD* (Lueck 1987), *TOMI* carries a suite of 6 types of environmental sensors (i) two large (1.2 cm) and two small (0.7 cm) airfoil probes (Osborn and Crawford 1980) for measuring two components of the cross-axial turbulent velocity shears, $(\partial w/\partial x, \partial v/\partial x)$; (ii) two fast *Thermometrics* FP07 thermistors sampled temperature and temperature combined with the temperature derivative (Mudge and Lueck 1994) to provide a high resolution temperature record; (iii) two impeller type current meters; (iv) three pairs of *Sea-Bird* SBE3 temperature and SBE4 conductivity sensors; (v) one *Sea-Bird* oxygen sensor and (vi) two side scan sonars for imaging bubble clouds and an echo sounder. These environmental sensors are summarized in table 3.1.

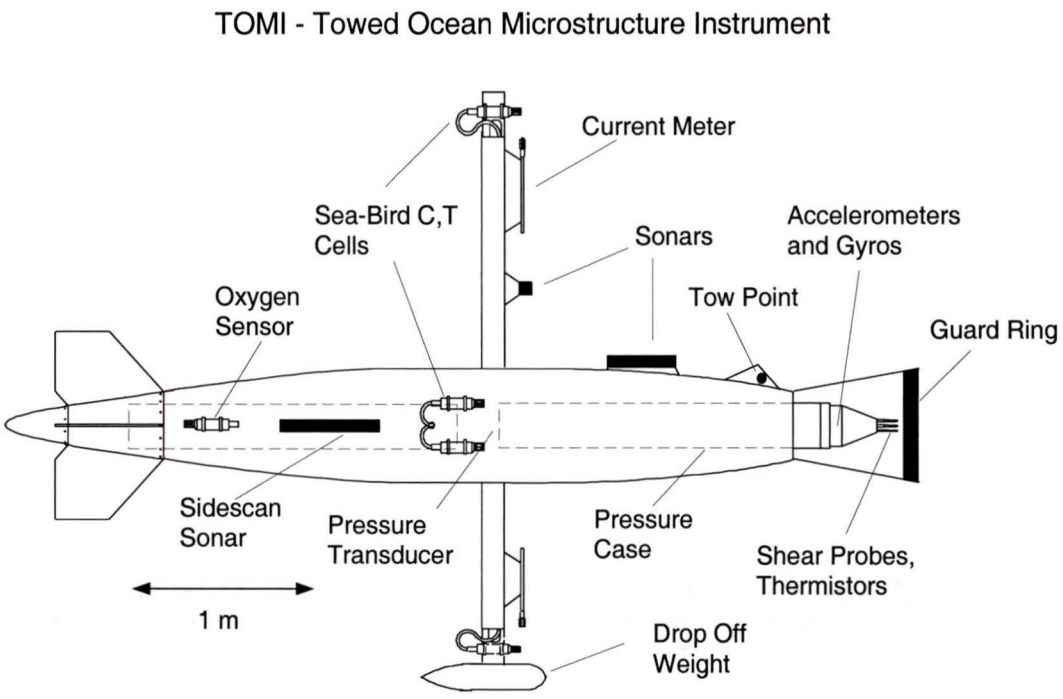

Figure 3.1: *TOMI* - The Towed Ocean Microstructure Instrument (diagram courtesy of Fabian Wolk)

TOMI is constructed from the wing tank of a fighter aircraft and contains two pressure cases, one fore and one aft, to house the electronics. The hull is made to be nearly neutrally buoyant by filling with syntactic foam. A guard ring at the front protects the shear probes and thermistors which protrude from the pressure case and a set of fins at the rear aids stability during towing. Communication with the ship is via a nearly neutrally buoyant six conductor kevlar cable. A paravane was used to move the instrument to starboard, out of the wake of the ship. Unlike *HOTDAD*, *TOMI* has a teardrop shaped mast extending 1.5 m above and 1 m below the centre line of the instrument which allows a local profile of temperature and salinity to be

Sensor	*Number*	*Physical Quantity*	*Sampling Rate*
Shear probe	2 × 1.2 cm, 2 × 0.7 cm	$\partial w/\partial x$, $\partial v/\partial x$	1024 Hz
FP07 Thermistor	2	T	128 Hz
FP07 Thermistor	2	$T + dT/dt$	1024 Hz
Current meter	2	U	128 Hz
SBE3 temperature probe	3	T	64 Hz
SBE4 conductivity probe	3	C	64 Hz
Oxygen probe	1	O_2	64 Hz
Sonar	1 forward, 2 side, 1 upward	bubble concentration	4 Hz

Table 3.1: Environmental sensors on *TOMI* during MBLII

measured providing a quasi-horizontal section of buoyancy frequency.

In addition to the major environmental sensors, *TOMI* comes equipped with a set of secondary sensors to measure body motions and depth. There are three orthogonal *Q-Flex* accelerometers to sample pitch, roll and heave at 1024 Hz, three *Systron Donner* gyros to measure rotation rates at 128 Hz, a *KVH* fluxgate compass and a *Keller* pressure transducer, sampled at 64 Hz. GPS data is recorded simultaneously by a feed from the ship's navigation system.

3.2 Instrumentation on the R/V *Wecoma*

The *Wecoma* had an onboard logging system, *XMIDAS*, to record navigational information and basic meterological data. *XMIDAS* recorded positional information each minute from 4 different systems, including Loran C, but unfortunately was neither equipped with differential GPS, nor recorded the satellite data which would have enabled differential post-processing. Heading information, longitudinal and tranverse speeds through the water, wind speed, wind direction and sea surface temperature were also recorded.

The *Wecoma* was also fitted with a hull mounted 300 kHz narrowband Acoustic Doppler Current Profiler (ADCP) made by RD Instruments. The ADCP was downward looking in a four beam Janus configuration. The pulse length was set at 4 m and there were 64 bins of size 2 m giving a total profile depth of 128 m. The instrument range-gates the backscatter to produce a weighted average over a Bartlett window. The effective filter, which is a convolution of the 2 m and 4 m gates, has a transfer function

$$T_f(k) = \mathrm{sinc}\,(\pi a k)\,\mathrm{sinc}\,(\pi b k)$$

where a is the vertical bin size, b is the pulse length and k is the vertical wavenumber (cpm) of the scattered acoustic spectrum (Chereskin *et al.* 1987). Velocity profiles were recorded every minute and contained an ensemble average of 80 pings.

3.3 Meterological measurements

Meterological measurements were provided by Jim Edson (personal communication, 1997) using the WHOI Direct Co-variance Flux System and included both bulk flux (Large and Pond 1981) and eddy co-variance calculations. The instrumental set-up is described in detail in Edson *et al.* (1998).

Measurements from ships are problematic for a number of reasons. Sea spray can contaminate the temperature probes and mechanical failure due to corrosion can also occur. In addition, flow distortion around the ship and the problems of correcting for platform motion in eddy covariance techniques (as with *TOMI*) need to be resolved.

The meteorological package on the *Wecoma* consisted of *Solent* three-axis sonic anemometer-thermometers, *Väisälä* relative humidity-temperature sensors with a radiation shield and an *Ophir* infrared hygrometer for making direct estimates of the latent heat flux. The sonic anemometer and *Väisälä* units were deployed at 5.6, 11.5 and 11.3 m above mean sea surface.

Data were provided in 10 minute averages, although due to the noisiness of the direct covariance measurements, 30 minute averages were the minimum that Edson *et al.* (1998) found that they could use in order to obtain reasonable statistics. Comparison with data recorded simultaneously on the R/V *FLIP* during the MBL II experiment revealed the ship based flux estimates to be underestimates by 15% after this averaging. The *Ophir* infrared hygrometer did not work very well during

the experiment and only limited data were available from it.

Chapter 4

Background oceanographic and meteorological conditions

The R/V *Wecoma* covered a broad area during the cruise bounded by 36°51′-35°38′ N 122°48′-121°52′ W. However, most operations were conducted in the vicinity of the R/V *FLIP* and so *TOMI* tows were concentrated around 36°39′ N 122°32′ W (Figure 4.1). Operations were interrupted twice during the cruise, firstly JD111-113 due to damage sustained in a storm on JD109 and secondly on JD118 due to a broken capstan. Both caused time to be lost returning to Monterey Bay for repairs.

The MBL II experiment was characterized by a storm on JD108-109 when winds gusted at up to 20 ms^{-1}, followed by more steady, moderate winds of around 10 ms^{-1} from JD112-116. During the storm there was no rotation of the wind vector as the wind blew steadily to the SE. Subsequent winds were variable with some short periods of low 1-2 ms^{-1} winds and some periods of fog. The storm appeared to generate strong horizontal density gradients. CTD profiles (courtesy of D. Farmer) taken soon after the storm show a well mixed layer to 60m. Casts made through the following days show two distinct well mixed layers as night time convection following the storm only mixed down to between 10 and 20 m. Sea surface temperature remained fairly stable at around 13°C during the cruise but was depressed by 2°C just prior to the storm. The mean surface salinity through the cruise was 32 psu. Air temperature fluctuated

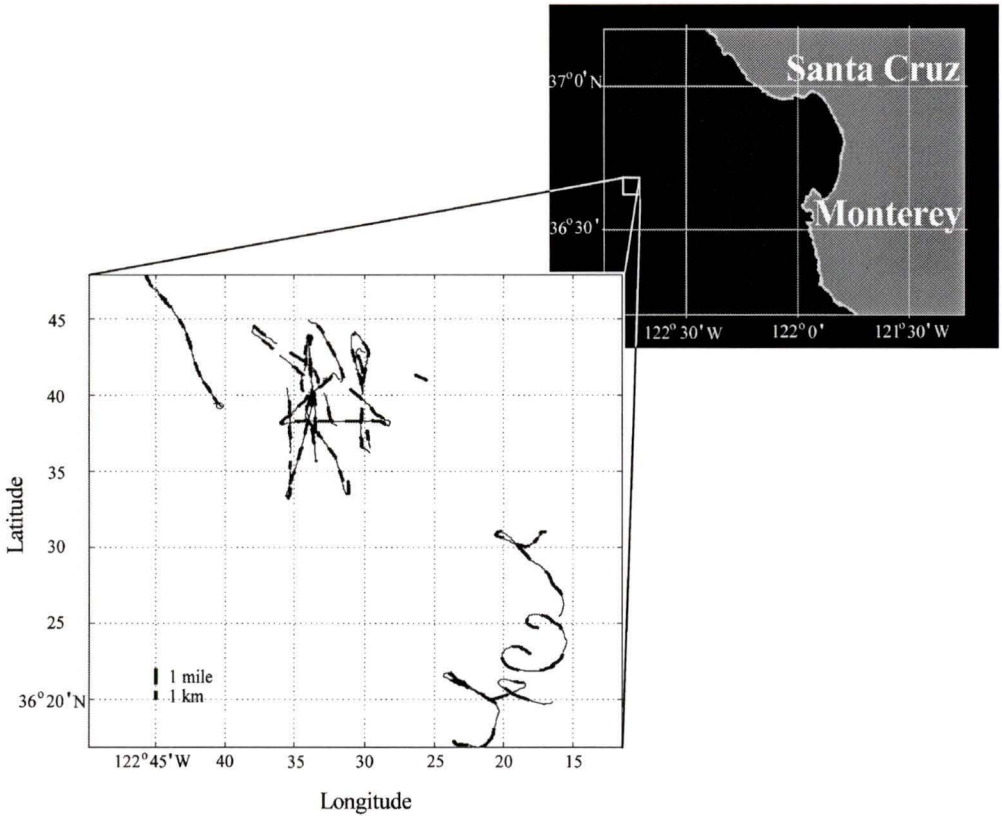

Figure 4.1: Location of *TOMI* tows during the MBL II experiment.

around 11°C in the first half of the experiment and dipped to 9°C before a warming trend starting on JD114 raised the air temperature to around 14°C. Maximum surface heat fluxes of 250 Wm^{-2}, from the ocean to the atmosphere, occurred during the storm but were otherwise less than 100 Wm^2.

4.1 Tow 1- JD116 00:09-18:06 UTC

The tow track for JD116 and sea surface temperature (sst) along it are shown in Figure 4.2.

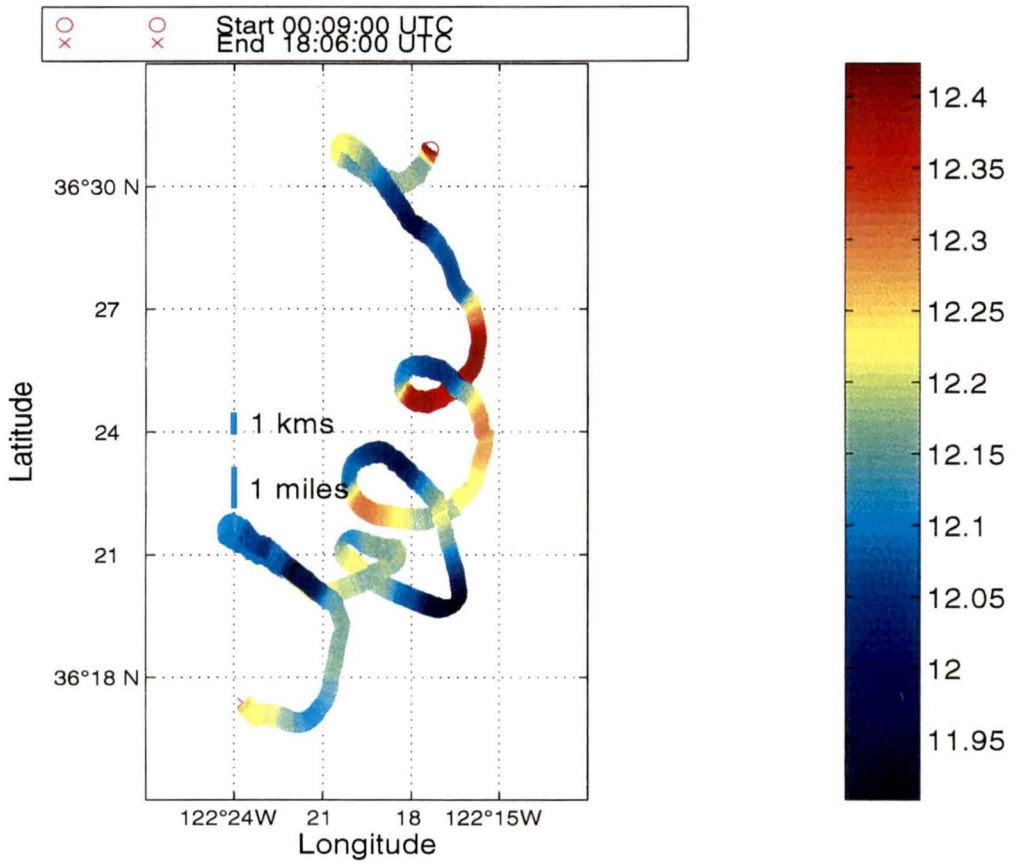

Figure 4.2: Sea surface temperature and tow track, JD116 00:02-18:06 UTC.

During this period the *Wecoma* was tracking and circling the instrument *DARSI* operated by D. Farmer. There are evidently significant changes in the temperature field in both time and space. Satellite imagery during this period reveals significant mesoscale activity in the area. Fronts (such as the one at 36°25′ N 122°19′ W) are

clearly evident. Wind work at 10 m ($E_{10} = \tau U_{10}$) height varied from 1-3 Wm^{-2}, the air temperature was 1-1.5°C below the sea surface temperature and a surface buoyancy flux of 1.5×10^{-7} WKg^{-1} was supported until JD116.58 (07:00 PDT) when surface warming due to incoming solar insolation reversed the direction of the flux (Figure 4.3).

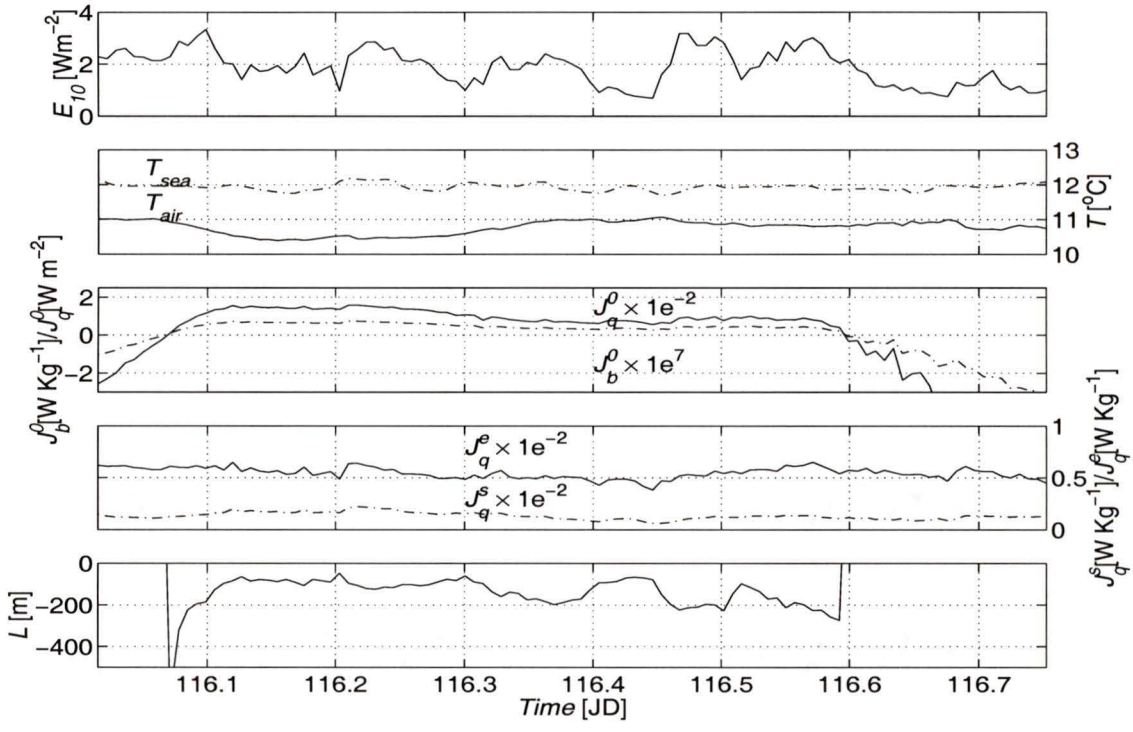

Figure 4.3: Meteorological summary for JD116-116.75 (00:09-18:06 UTC) (a) wind work at 10m height, (b) sea surface and air temperatures, (c) buoyancy flux and total heat flux, (d) latent and sensible heat fluxes, (e) Monin-Obukhov length.

As discussed in chapter 2, the Monin-Obukhov length is a measure of the depth at which mixing by wind stress, u_*, is as effective as mixing by buoyancy forcing, J_b^0.

When the mixed layer depth is less than L, wind mixing dominates over buoyancy forces. Figure 4.3(e) shows that this length grew from 100m depth to 300m, much greater than the mixed layer depth and so the mixed layer was entirely dominated by wind forcing before the direction of the surface flux reversed at JD116.59 (06:16 PDT).

4.2 Tow 2 - JD122 05:35-15:32 UTC

The second tow track and sst are shown in Figure 4.4.

During this time, operations were being conducted around *FLIP*. Fronts were less obvious during this tow except in the region around 36°38.4′ N,122°26.6′ W and wind work was an order of magnitude lower than the first tow (Figure 4.5).

The night time air-sea temperature difference was smaller than the first tow. A small positive buoyancy flux was supported through the night. The lower wind forcing is reflected in the much smaller Monin-Obukhov length but again the reversal in sign of the Monin-Obukhov length and of the buoyancy flux is clear with the increase in stratification during surface warming.

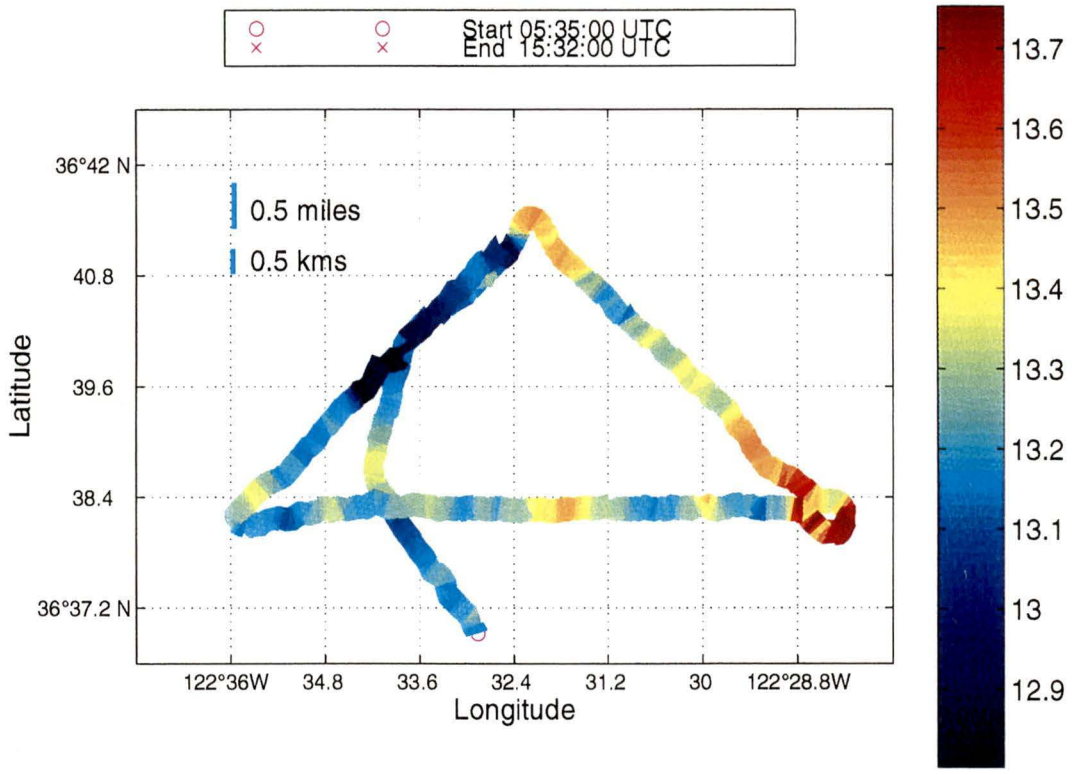

Figure 4.4: Sea surface temperature and tow track 2, JD122 05:35-15:32 UTC.

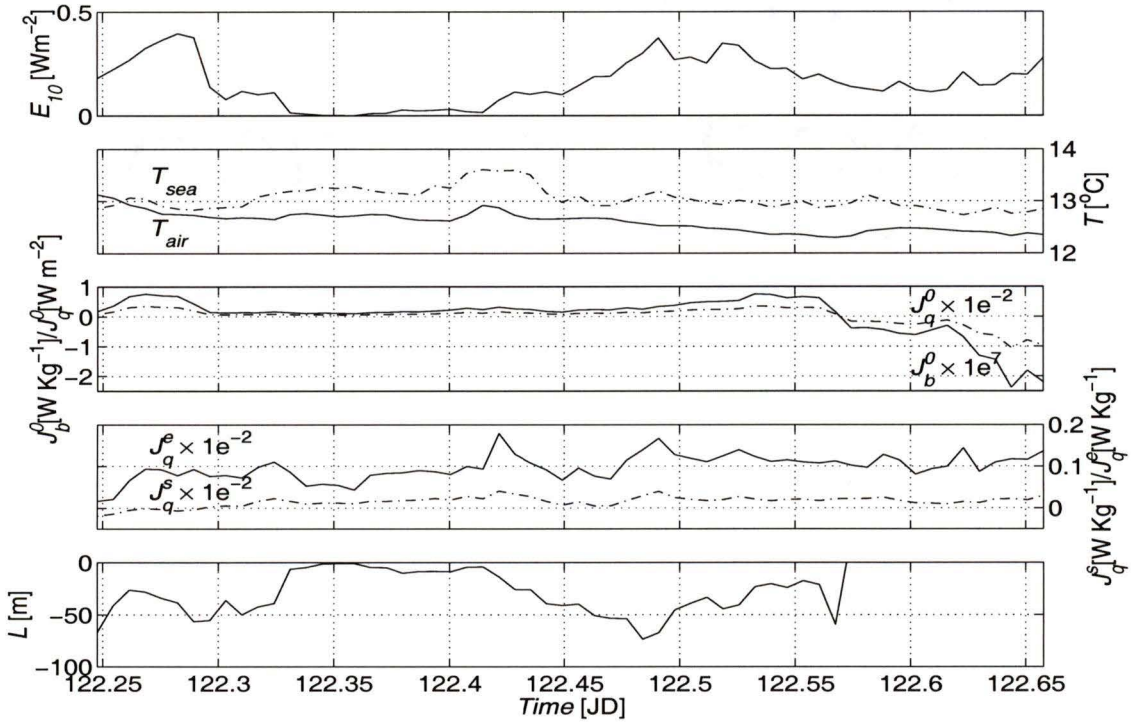

Figure 4.5: Meteorological summary for JD122.23-122.66 (05:35-15:32 UTC) (a) wind work at 10m height, (b) sea surface and air temperatures, (c) buoyancy flux and total heat flux, (d) latent and sensible heat fluxes, (e) Monin-Obukhov length.

Chapter 5

Data processing

5.1 Shear

Shear was calculated from 5 minute ADCP velocity averages smoothed over 10 m (5 bins) in the vertical. To ensure that there were no significant biases in the data caused by the misalignment of the ADCP on the ship, the error velocities were checked and found to approximate well to a normal distribution with zero mean over the 5 minute average. The co-variance matrix indicated that frequency and wavenumber space observations were independent of each other and spectra in both wavenumber and frequency space were also found to be white.

It was then necessary to ensure that the 10 m shear was adequately resolved, meaning that the averaging process had to reduce signal noise to lower levels than the shear signal we were seeking to examine. The transfer functions of the first difference operator and the 5 point running mean in wavenumber space were calculated and combined with a five point running mean in frequency space to give a variance weighting of 0.0039. That is, the combined effect of the two filters was to reduce variance to 0.0039 of that of a white spectrum. The half power point in wavenumber space occured at 0.045 cpm. RD Instruments (personal communication 1997) give

the RMS error in velocity as:

$$E_{RMS} = \frac{1.6\times10^5}{fd\sqrt{n}}$$

where f is the frequency of the RDI unit (307200 Hz), d is the cell depth size (2 m) and n is the number of pings (80 per minute). Hence a 1 minute average has a theoretical $E_{RMS} = 0.0291$ ms^{-1}. The variance weighting reduces the RMS shear to 1.14×10^{-4} s^{-1}. All our results are at least an order of magnitude above this level.

The shear layer was examined for evidence of an inertial response. At the latitude of the experiment, 36°N, the inertial period is $T_\tau = 12/\sin(36^o) = 20.42$ hours. The mean velocity was removed from each profile to remove ship speed and any mean current. Profiles were then averaged over 10 minutes and represented as a complex quantity, $u + iv$. The layer of peak shear was then identified from the ADCP velocity records which permitted examination of the rotation of the shear vector through time.

5.2 Calculation of TKE

The dissipation of turbulent kinetic energy (TKE), ϵ, is calculated by integrating the airfoil probe measured velocity shear spectrum and is given by:

$$\epsilon = \frac{15}{2}\nu\overline{\left(\frac{\partial w}{\partial x}\right)^2}$$

where ν is the kinematic viscosity. This procedure assumes isotropy of the turbulence and so should only be strictly applied to high Reynolds' number flows. Equivalently,

we could have used $\partial v/\partial x$.

The spectra were calculated over 5 minute periods from 4 s blocks of data (equivalent to approximately 5 m of tow at 1.25 ms^{-1}), half overlapped and ensemble averaged to improve their statistical significance. Removal of spikes was carried out as described in Wolk (1997) in which the rectified signal is compared to the heavily smoothed rectified signal and where the raw signal exceeds the local value of the smoothed signal by more than a specified amount, the points are replaced by the local mean. The shear probes act as low pass filters due to their finite size so Ninnis' (1984) high wavenumber correction was applied to account for this. Details of the procedure can be found in appendix B.

In order to avoid high wavenumber noise contamination but ensure that the universal shear spectrum (Nasmyth 1970) was sufficiently resolved, an iterative curve fitting routine was used to compare the variance of the measured signal over a limited range of wavenumbers, k, with that of the universal spectrum over the same range of wavenumbers. The level of the universal spectrum was estimated from the integral of the measured spectrum over the waveband k. The procedure was repeated until the variance of the measured spectrum over k agreed with the variance of the universal spectrum integrated over that waveband to within 5%. Further details can be found in appendix C.

Body vibrations are a frequent source of contamination of the high frequency

shear signal (Moum and Lueck 1985). As *TOMI* was fitted with accelerometers in 3 co-ordinates, the accelerometer spectrum was calculated over the same time interval as the shear spectrum and coherent accelerations removed (see appendix D).

As discussed in chapter 2, the amount of data required to make dissipation estimates from the spectral technique can be larger than the size of the patch when turbulence is weak. The technique of Yamazaki and Lueck (1990) uses point by point calculation of the dissipation rate which is then averaged over a number of points equivalent to ten Kolmogorov lengths to ensure statistical independence of the estimates. This technique was used to examine the effect of strong stratification on dissipation estimates and was not the usual technique for calculating dissipation.

5.2.1 Error estimation

Errors in the calculation of the dissipation can arise from a number of sources. As mentioned above, contamination of the shear signal by mechanical vibrations can be a problem though this has been minimized by the removal of coherent signals. It is possible that, because the accelerometers were mounted about 0.3 m to the rear of the centre of *TOMI*, whilst the shear probes project from the front, certain motions were not registered coherently by the sensors. However, it is likely that other sources of error are larger.

The conversion of the shear signal into physical units, $\partial w/\partial x$, is dependent on an accurate knowledge of the flow speed where it enters as U^2. Since the calculation

of the dissipation is $\overline{(\partial w/\partial x)^2}$, any error in U will be 4 times as large in ϵ. A likely value for the r.m.s. error in U is $\pm 5\%$ which means a $\pm 20\%$ error in ϵ.

In addition to this error, there are both systematic and random errors in the calibration of the probe sensitivity. The repeatability of the calibration process is estimated by Wolk (1997) to be $\pm 5\%$. Whilst the systematic errors are very difficult to estimate, Oakey (1982) suggests that the systematic errors may double the random error so that the total error in the probe sensitivity of $\pm 10\%$.

Ninnis (1984) estimates that the error introduced in the recovery of lost variance from the spatial smoothing of the probe amounts to $\pm 5\%$ at the dissipation rates typical of the those measured here.

Errors from the assumption of isotropy at low Reynolds' numbers and other random and systematic errors such as those related to the temperature sensitivity of the probe (see Wolk (1997), appendix C) leads to the conclusion that the estimates of ϵ are accurate to within a factor of 2.

5.3 Calculation of N^2

TOMI's three pairs of *Sea-Bird* temperature probes and conductivity cells allow a continuous local horizontal profile of buoyancy frequency, N^2, to be calculated. The buoyancy frequency is given by:

$$N^2 = g\left[\alpha\left(\frac{dT}{dz} + \gamma\right) - \beta\left(\frac{dS}{dz}\right)\right]$$

where $\alpha = -\rho^{-1}(\partial\rho/\partial T)_{p,S}$ is the coefficient of thermal expansion, $\gamma = g\alpha T/c_p$ is the adiabatic lapse rate and $\beta = \rho^{-1}(\partial\rho/\partial S)_{p,T}$ is the coefficient of saline contraction.

5.3.1 Error estimation

From looking at a particularly quiescent section in which the temperature and salinity remained approximately constant, estimates can be made of the random errors introduced into the temperature and conductivity signals. Systematic errors arising from calibration should be small for these sensors and the mean drift in the temperature probes between pre- and post-cruise calibrations was 6×10^{-4}°C. It seems reasonable to assume a linear drift in the probe calibrations throughout the cruise and taking this into account, Wolk (1997) estimates the error in N^2 to be $\pm 2 \times 10^{-6}$ s^{-2} over a 5 minute average.

5.4 Calculation of temperature gradient skewness

The temperature ramps which lead to skewness in the derivative are low frequency, $O(10^{-2}$ Hz) (Thorpe and Hall 1980), whilst high frequency turbulence is isotropic and hence unskewed. The centre *Sea-Bird* temperature sensor samples at 64 Hz and so was resampled at 1 Hz. The temperature signal was then first differenced and then converted to a spatial derivative using Taylor's hypothesis:

$$\frac{\partial T}{\partial x} = \frac{1}{U}\frac{\partial T}{\partial t}$$

where U is the speed of the instrument through the water. Since the tow speed was much greater than the mean flow speed, a "frozen eddy" hypothesis was used to look at the sign of $\mathtt{S_k}$ (Thorpe *et al.* 1991).

Orientation with respect to the shear was calculated by finding the shear direction for the ADCP bin which coincided with *TOMI*'s depth and using the heading information recorded in the ADCP. The ADCP automatically corrects for misalignment of the beams.

5.4.1 Error estimation

Potential errors arise from the positioning of *TOMI* in relation to the the ADCP. Errors can come from two areas, firstly depth and secondly time lag.

In the first case, the ADCP records in bins from the depth at which it is positioned on the hull of the *Wecoma*. The depth of the ADCP was given as 5 m (B. Wendler, personal communication 1998) but this depth is not accurately known and could be ± 0.5 m.

The pressure transducer on *TOMI* had an offset which was calculated as +2.07 m from deck test data. The pressure transducer is very precise but it is possible that the shear taken to be characteristic of *TOMI*'s depth could be wrong by 1 ADCP bin.

A more difficult problem to evaluate is the effect of the towing arrangement on our ability to synchronize the shear and data collected from the towed instrument.

TOMI was typically towed 200 m behind the ship and the paravane removed the vehicle some 40 m out to the side of the ship to avoid the wake. The difference in timing is relatively easy to account for if the assumption of the tow distance is correct and we know the ship speed. Typically this correction is 200 s. It is impossible to estimate the errors resulting from the displacement to the side of the ship however.

Following the return of the ship to Monterey Bay on JD111-112 for repairs, an error appeared in the ADCP which amounted to the clock being slow by 23 hr 50 min. This error was constant and can be accounted for to one minute through synchronizing the positional information recorded separately by the ADCP and the ship's logging system.

Chapter 6

Results

6.1 Frontal dynamics

A shear layer was clearly visible in the ADCP plots for tow 1 (Figure 6.1). There was a front at 36°25′ N 122°19′ W (Figure 4.2 which occurred at JD116.2 (Figure 6.1(b)). Here, cold water lay to the north west and warm water to the south east. Although the change was only approximately 0.3°C over a distance of about 300 m, the two water masses were clearly distinct and were both quite homogeneous in both temperature and salinity. The manifestation of the front in the surface temperature was clearly depicted in the shear which was strongly enhanced at the front and sloped with depth in a way consistent with the less dense, warmer water attempting to re-stratify by moving over the cooler, denser water (Figure 6.1(c)). The CTD cast taken through this layer at JD116.24 (Figure 6.2) showed this layer of warmer water with a temperature of 12.2°C overlying water of 11.4°C with a sharp interface between 16 m and 23 m depth.

If it was the re-stratification process which was generating the shear between the two layers, and the flow was close to thermal wind balance at the time of observation,

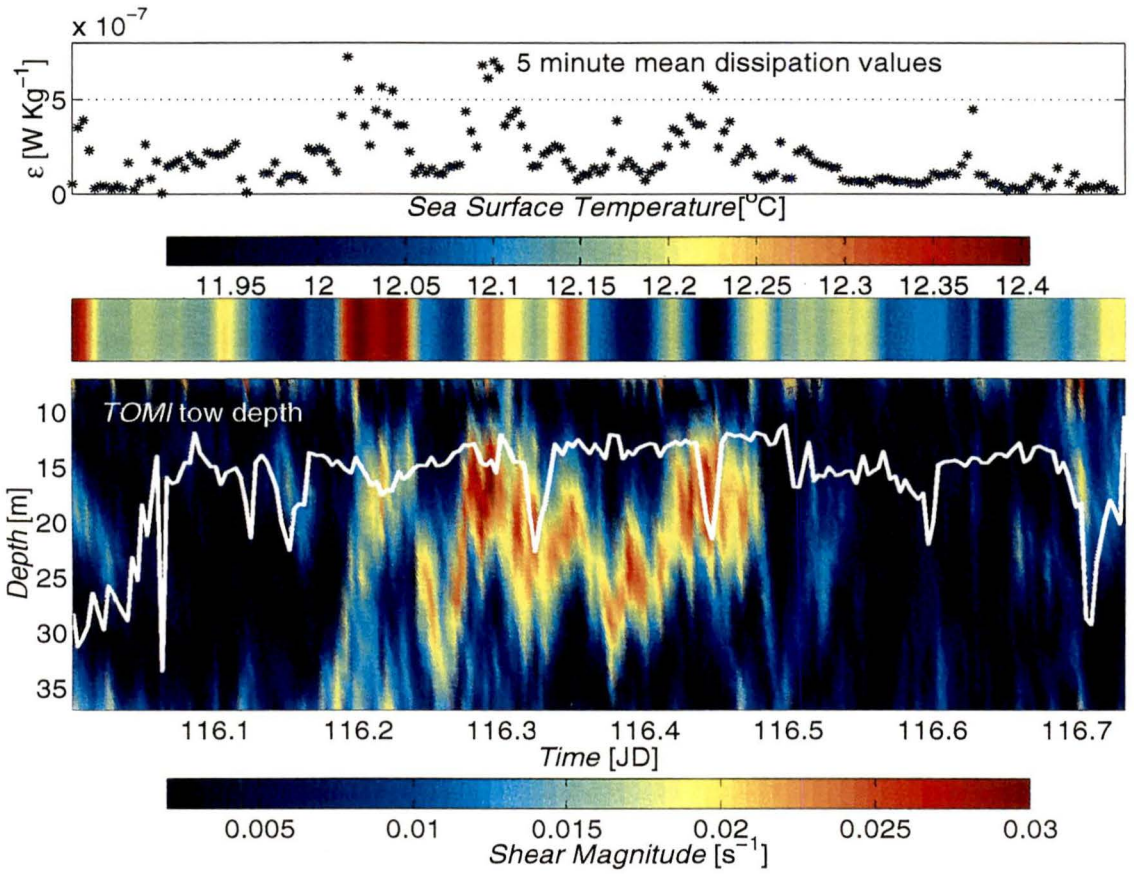

Figure 6.1: (a) Dissipation averages over 5 minutes (b) Sea surface temperature and (c) shear magnitude (interpolated 5 minute averages) from tow 1, JD116

then the shear should be approximated by

$$f_c \frac{dv}{dz} = \frac{g}{\rho_0}\left(\frac{\rho_2 - \rho_1}{\Delta x}\right) \tag{6.1}$$

$$f_c \frac{du}{dz} = \frac{-g}{\rho_0}\left(\frac{\rho_2 - \rho_1}{\Delta y}\right) \tag{6.2}$$

The Earth's rotation is considered important when the Rossby number, Ro, ($\equiv U/f_c L$, where U is the difference in velocity between the two layers and L is the e-folding length of the shear layer) is much less than 1. For typical values of $U = 0.2$ ms^{-1} and

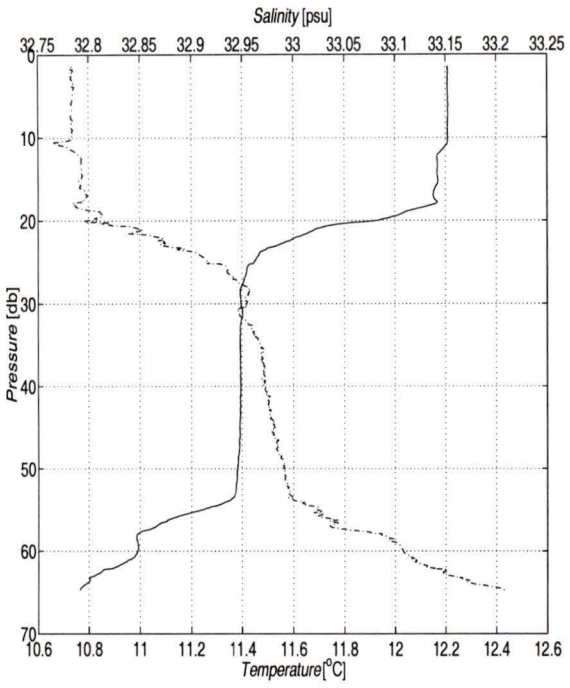

Figure 6.2: Temperature (solid line) and salinity (-.-) profiles through the shear layer of tow 1, JD116.24

$L = 6$ Km, we have $Ro = 0.16$. The observation of a high shear layer in the ADCP data over a period of several days prior to tow 1 also suggested that the timescale of evolution for the layer was likely to be several inertial periods and so the Earth's rotation would have an effect. Using the measured values of the density of the cooler layer, $\rho_1 = 1025.5649$ Kg m^{-3} and for the warm layer, $\rho_2 = 1025.5234$ Kg m^{-3} and taking $\Delta y = \Delta x = 400$ m, $f_c = 1 \times 10^{-4}$ s^{-1} with $\rho_0 = 1025$ Kg m^{-3}, gives the total shear, $((du/dz)^2 + (dv/dz)^2)^{1/2} \approx 2 \times 10^{-2}$ s^{-1}. As can be seen, this is in excellent agreement with the magnitude of the shear in the front, estimated from the ADCP data (Figure 6.1(c)).

6.2 Shear, stratification and dissipation

6.2.1 Tow 1

The association of increased temperature variance with crossing the front and entering the warmer surface layer, whilst low temperature variance appeared to be associated with the cooler waters, is an interesting feature of this dataset (Figure 6.3(a)). The shear data recorded by the ADCP at the depth at which *TOMI* was being towed makes it clear that the increase in temperature variance was associated with enhanced levels of shear. Furthermore, the high shear levels coincided with both high levels of dissipation and higher stratification (Figure 6.3(b-c)). From a comparison of *TOMI*'s depth with the shear and CTD profiles, it seems clear that *TOMI* was often towed through the shear layer which separated the two water masses.

The shear layer was examined for evidence of inertial rotation as velocity profiles suggested some clockwise rotation of the velocity vector with depth which would be consistent with the zero order mode of a downward propagating near-inertial wave (Leaman and Sanford 1975; Gill 1982). Although inertial activity had been detected several days previously, no evidence of rotation could be found during this period and so it is concluded that the shear layer is unrelated to inertial activity.

Gradient Richardson numbers calculated along the tow track show that Ri_g was maintained below 0.25 for the portion of tow 1 associated with the high shear (Figure 6.3(d)). An increase in stratification accompanied the increases in shear levels

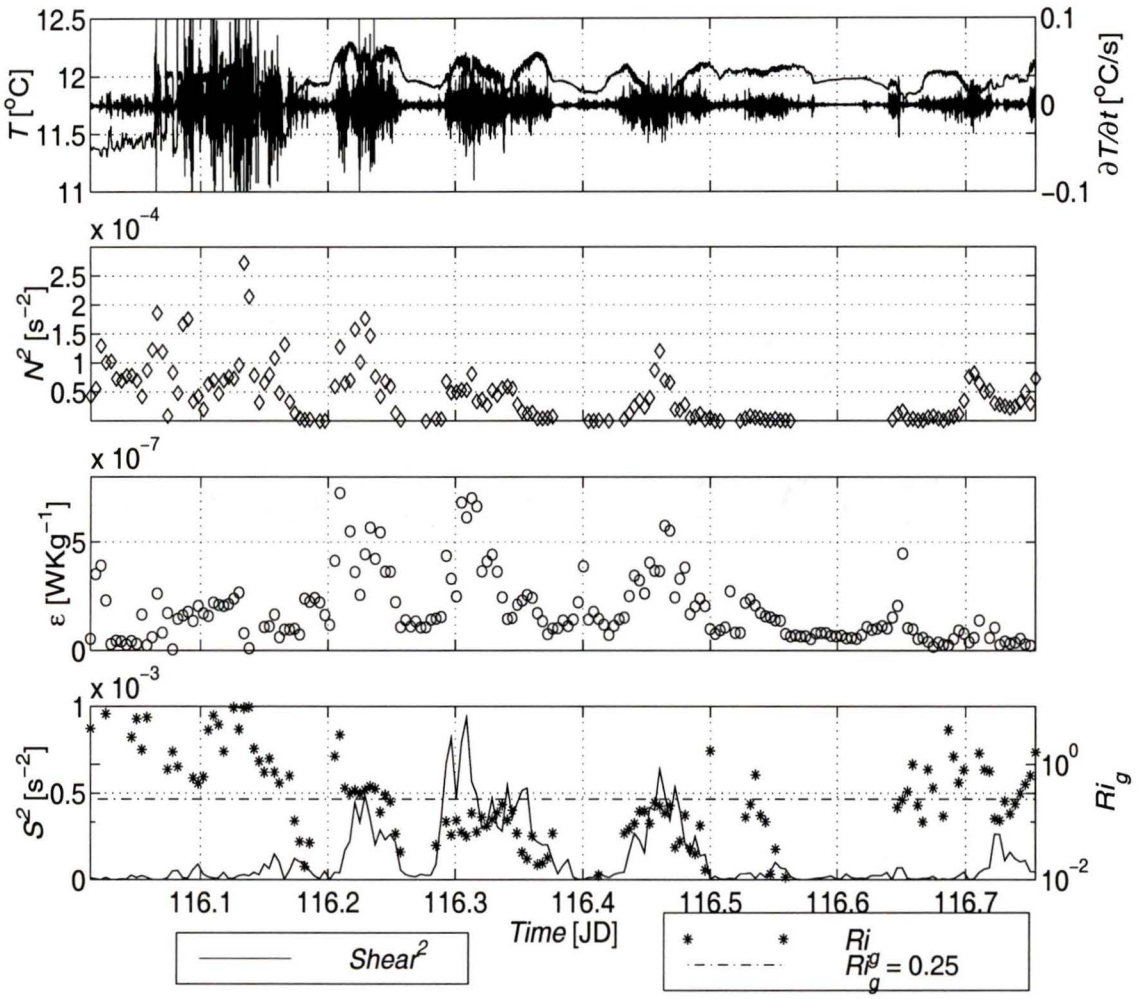

Figure 6.3: Summary of results from tow 1 (a) temperature and rate of change of temperature (b) 5 minute mean buoyancy frequency squared (c) 5 minute mean dissipation (d) 5 minute mean shear and gradient Richardson number.

and appears to have dominated slightly, actually raising Ri_g. The relationship between shear and stratification is made clear in figure 6.4 with the clustering below $Ri_g = 0.25$. No clear trend is visible to correlate the intensity of the dissipation with Ri_g nor is there any clear relationship between dissipation levels and temperature variance. In the latter case it might be remarked upon that although large temperature variances were sometimes seen at low dissipation rates, high dissipation rates were never associated with low temperature variance (Figure 6.5).

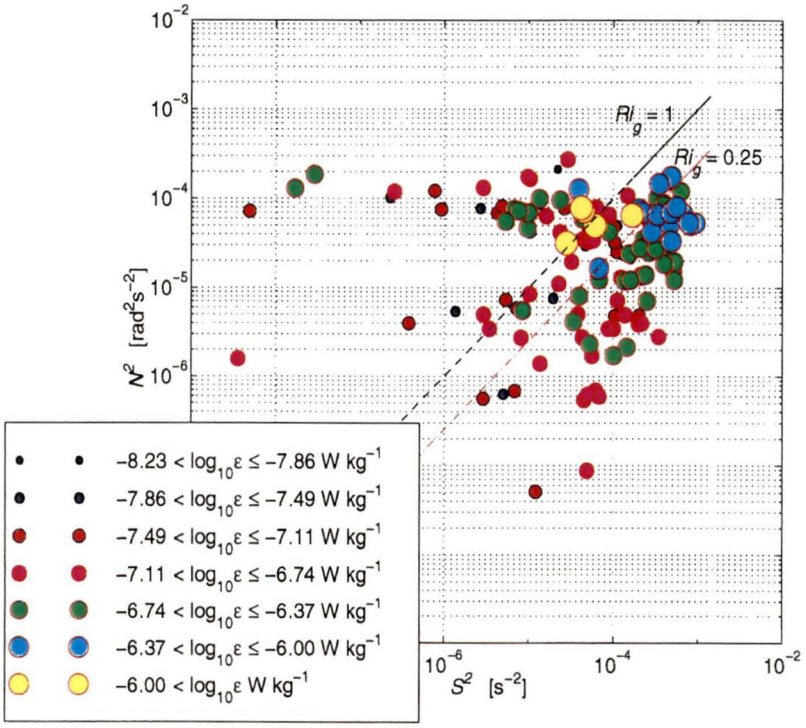

Figure 6.4: Shear, stratification and dissipation, tow 1, JD116. Larger circles indicate higher levels of dissipation.

Despite the evidence for shear instability, temperature gradient skewness did not

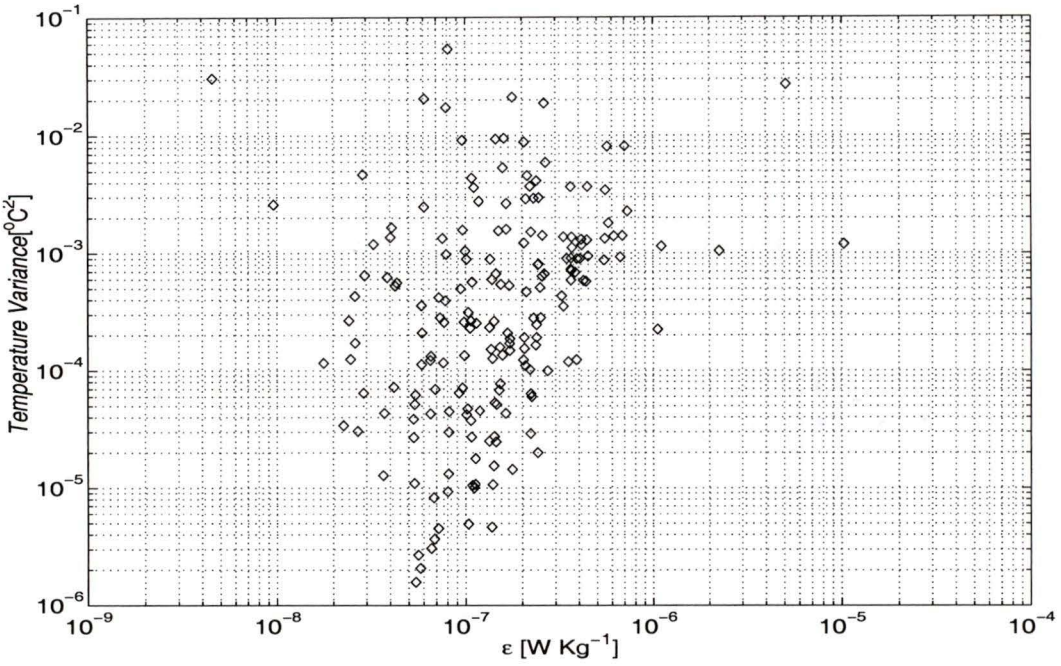

Figure 6.5: Dissipation and temperature variance, 5 minute means, tow 1

follow the sign convention of Gibson *et al.* (1977). No correlation was apparent between the tow angle and the sign of the skewness nor between the skewness and any other measured parameter. Additionally, there was no visual evidence from the temperature records of the type of ramp-like structure which is associated with a skewed temperature gradient and with Kelvin-Helmholtz type instabilities.

Calculation of the buoyancy Reynolds' number, Re_b, produces values of $O(10^4)$ and suggests that the turbulence was isotropic over some range of the velocity spectrum (Figure 6.6). In fact almost all the values of Re_b in tow 1 are greater than 200 which, as mentioned in chapter 2, is the level which Gargett *et al.* (1984) found to be the criterion for stratification to cause noticeable anisotropy in the inertial sub-range.

There is evidence in this figure that the lower Richardson numbers are also the most energetic and isotropic, as would be expected.

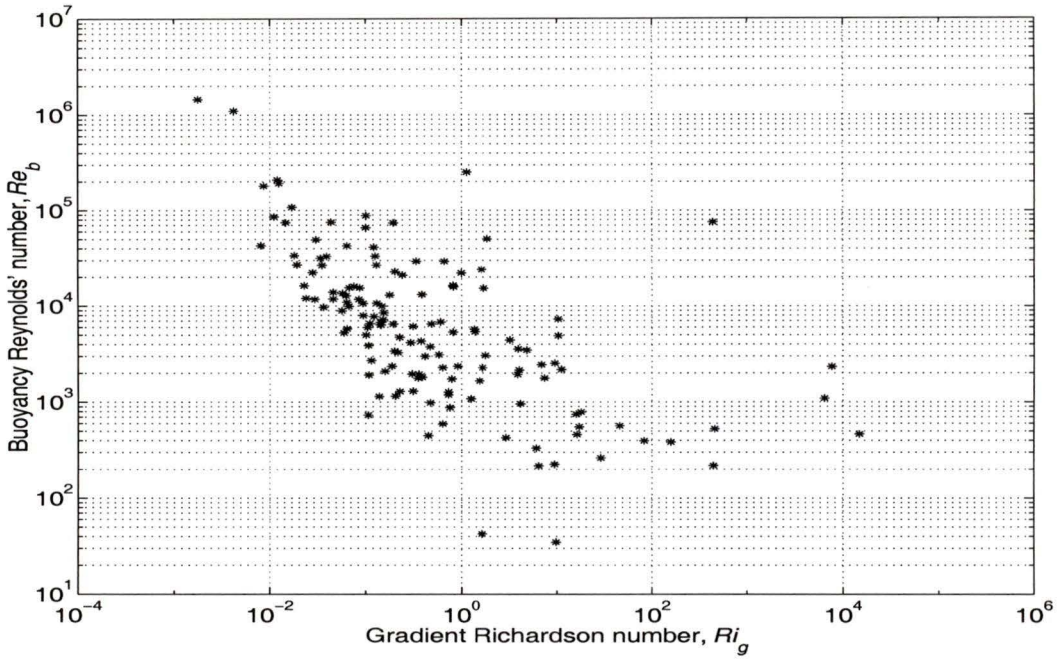

Figure 6.6: Gradient Richardson numbers and buoyancy Reynolds' numbers, tow 1. Low Richardson numbers have higher buoyancy Reynolds' numbers implying greater isotropy and higher energies.

Following Ivey and Imberger (1991) and Stacey *et al.* (1997), the data were plotted in the phase space of the turbulent Froude number, Fr_t, and turbulent Reynolds' number, Re_t. A comparison of the data from tow 1 with the data from both Ivey and Imberger (1991) and Stacey *et al.* (1997) shows that the data from tow 1 covers the same phase space as that of Stacey *et al.* (Figure 6.7). Contrary to the findings of Gargett *et al.* (1984), this implies that some of the data may be slightly anisotropic.

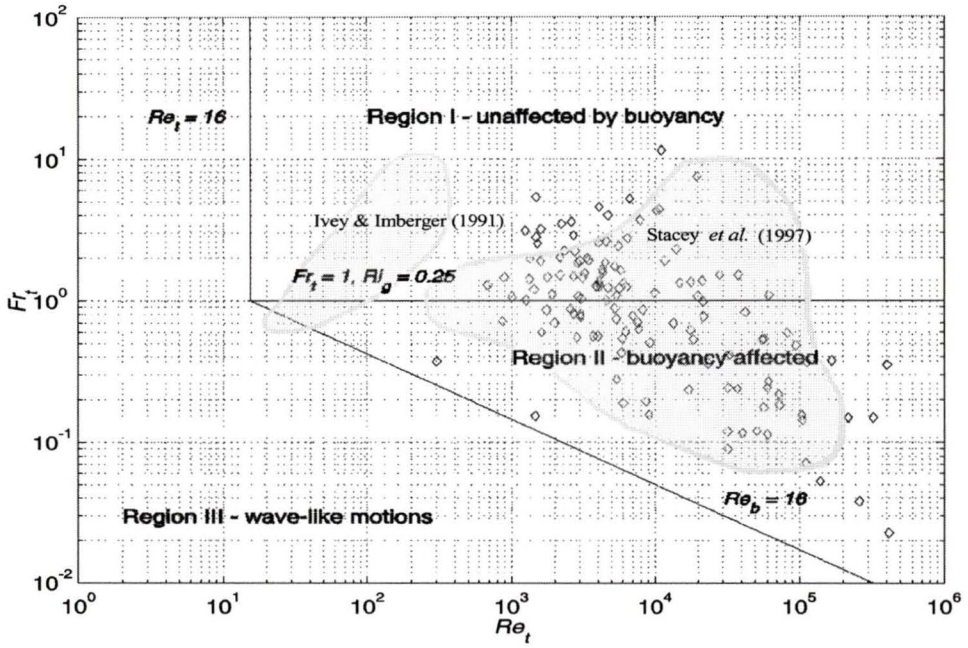

Figure 6.7: Turbulent Froude numbers and turbulent Reynolds' numbers, tow 1, using the phase spaces defined by Ivey and Imberger (1991). Shaded regions approximate the coverage of data from Ivey and Imberger (1991) and Stacey *et al.* (1997).

The eddy coefficient for density, K_ρ, was calculated using the parameterization of Osborn (1980),

$$K_\rho = \Gamma \frac{\epsilon}{N^2} \tag{6.3}$$

where $\Gamma = Rf/(1 - Rf)$ is known as the mixing efficiency. Using the argument that $Rf \leq 0.15$, Osborn (1980) set $\Gamma \leq 0.2$ and the value of $\Gamma = 0.2$ was used here. Again the effect of the increase in stratification dominated over the increase in shear and turbulence, as minimum values of K_ρ ($O(10^{-3})$ m^2s^{-1}) coincided with the regions of highest stratification, despite the elevated levels of dissipation. Peak values of K_ρ

($O(10^{-1})$ m^2s^{-1}) coincided with the weakest stratification and lowest dissipations.

The inverse of the echo intensity gradient magnitude reveals similar, though not identical, structures to the shear (Figure 6.8(c)). Echo intensity quantifies the amount of backscatter due to particles in the water, hence high intensity reveals accumulations of matter. Away from boundaries sediment loading does not contribute significantly to the backscatter and the echo intensity is indicative of the quantity of zooplankton. Using the gradient of the echo intensity helps to emphasise features in the water column but since it is the peak concentrations of zooplankton that we are interested in and not the areas of change, the inverse of the gradient has been taken to pick out those features. The peak values, which are also somewhat coincident with the high shear layer, are accumulations of biological particles. The front at JD116.2 and also at JD116.3 are clearly depicted in the upper 10 m of the echo intensity plot as thin regions extending down into the surface layer consistent with the concentration of particles in regions of convergence.

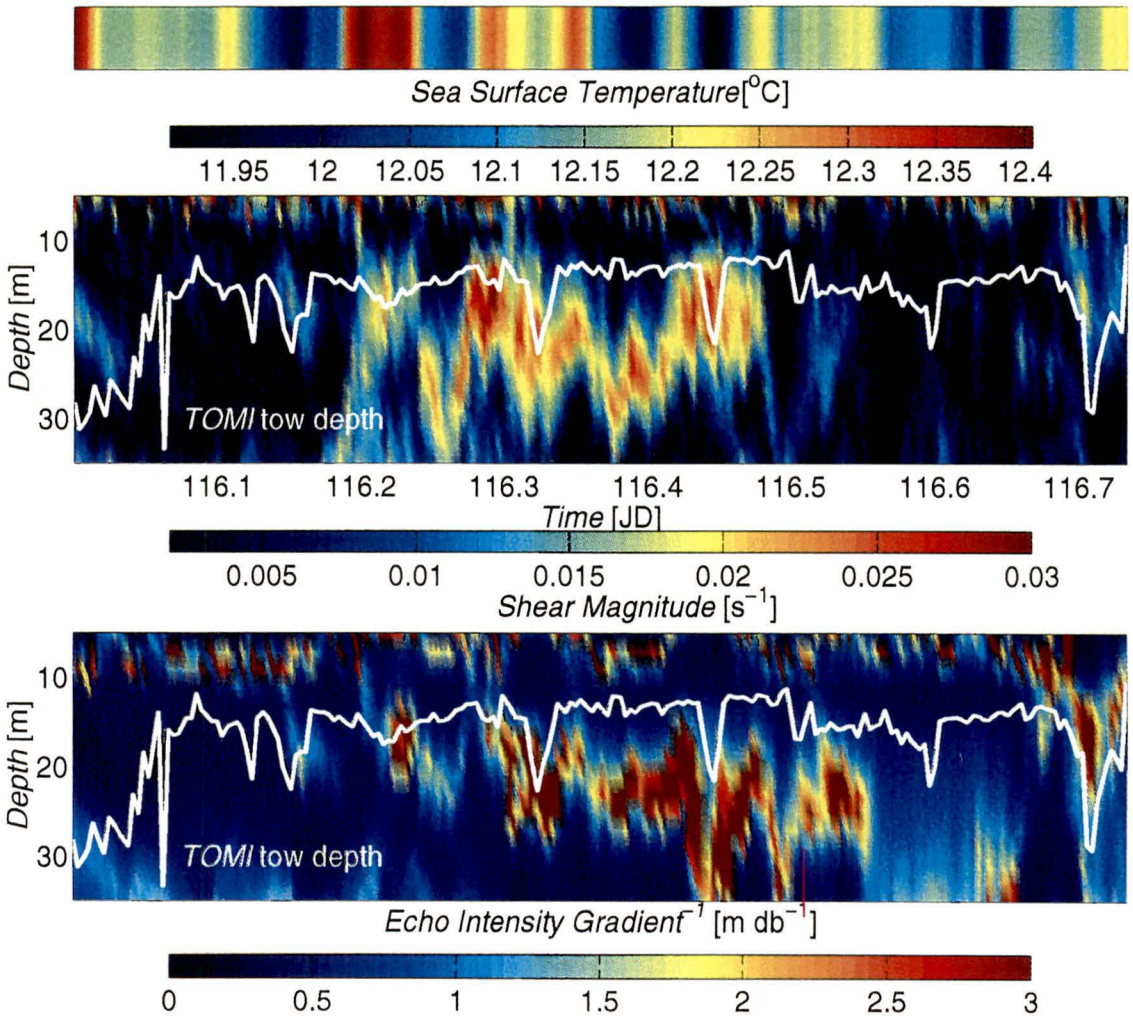

Figure 6.8: (a) Sea surface temperature (b) shear magnitude and (c) inverse echo gradient magnitude, tow 1

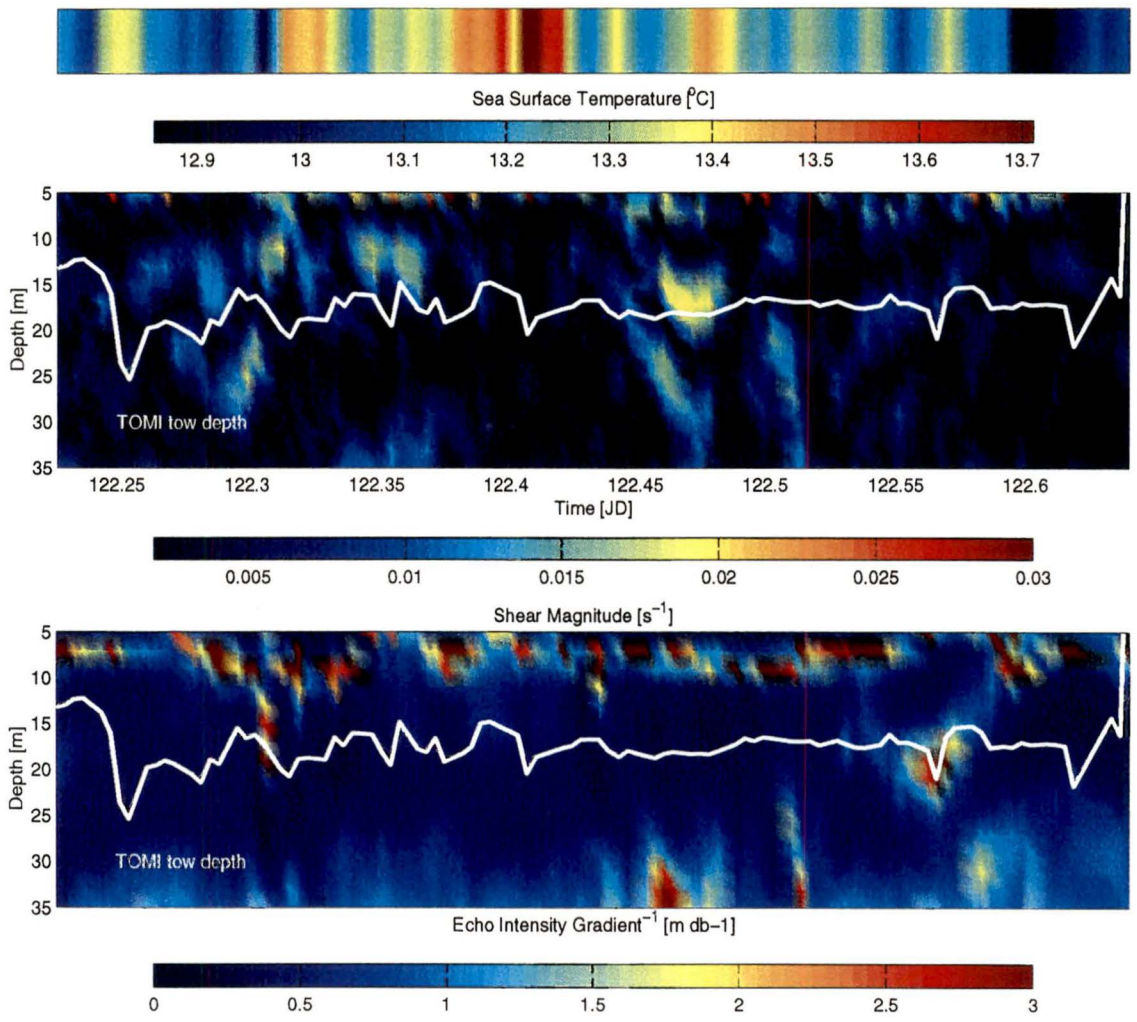

Figure 6.9: (a) Sea surface temperature (b) shear magnitude and (c) inverse echo gradient magnitude, tow 2

6.2.2 Tow 2

The second tow provided a rather different picture from the first. No distinct shear layers were visible (Figure 6.9) and the stratification was much greater (N^2 $O(10^{-3})s^{-2}$) than in tow 1 (Figure 6.10(b)). Large temperature anomalies were clearly evident, consistent with the exchange of water parcels in a strongly stratified environment where the temperature gradient is large, such as may occur with occasional overturns or internal wave activity.

Dissipation levels were lower ($O(10^{-8})$W Kg^{-1}), but still visually matched with bursts of more intense temperature variance (Figure 6.10(a,c)). As with the first tow, low temperature variance was rarely associated with high dissipation though the converse was not true. Gradient Richardson numbers were generally larger than 1 and always greater than 0.5 implying that the greater stratification dominated the shear and prevented any growth of shear instabilities. The distribution of points in S^2, N^2 space (Figure 6.11) shows that stability prevailed and there was no evidence of an increase in dissipation levels with the lower Richardson numbers. Again, the temperature skewness did not follow the Gibson *et al.* (1977) sign convention.

Turbulent Reynolds' numbers and turbulent Froude numbers show that the turbulence in tow 2 falls in the phase space which is strongly influenced by the stratification (Figure 6.13). Some of the very low values of dissipation ($\epsilon < 10^{-8}$W Kg^{-1}) have

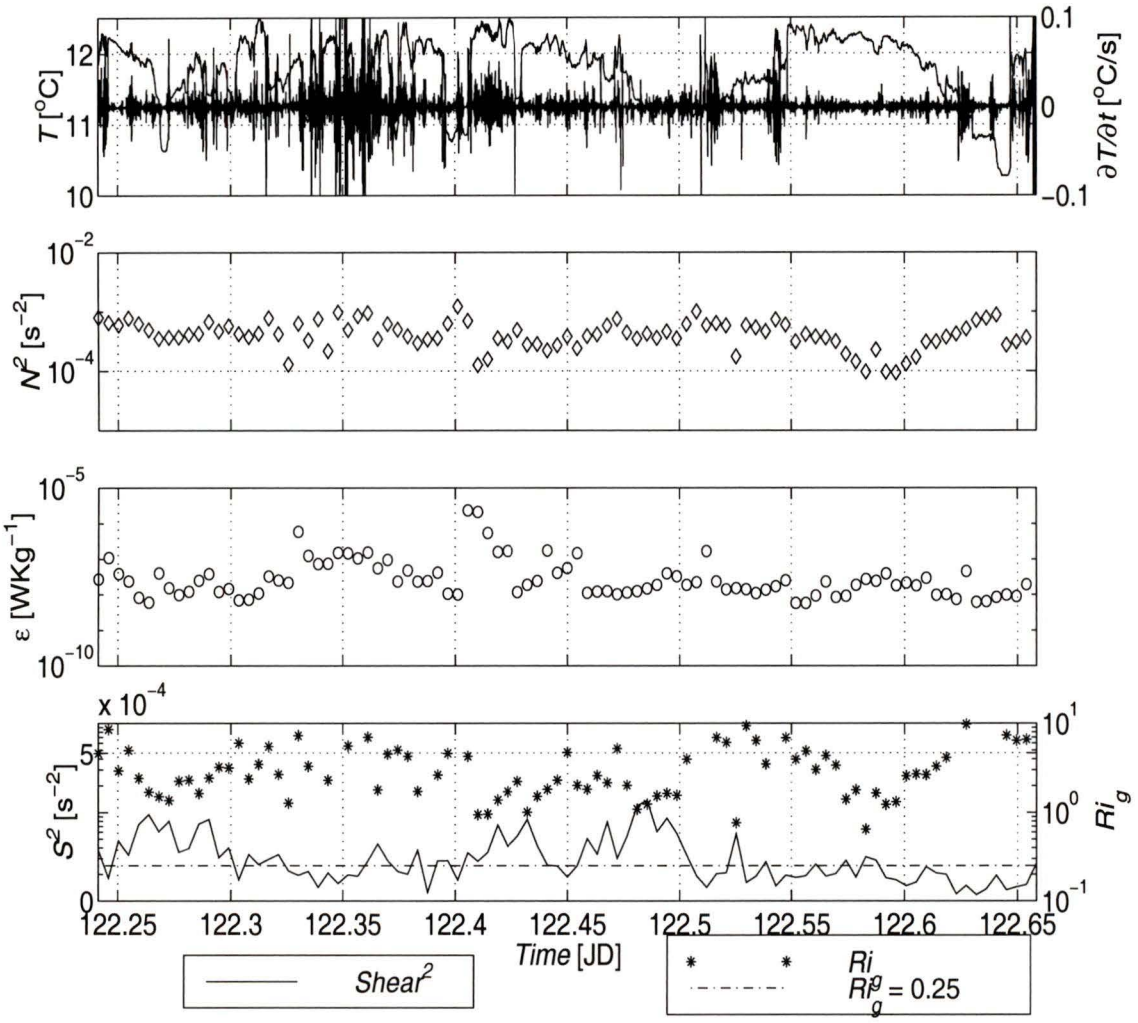

Figure 6.10: Summary of results from tow 2 (a) temperature and temperature variance (b) 5 minute mean buoyancy frequency squared (c) 5 minute mean dissipation (d) 5 minute mean shear and gradient Richardson number

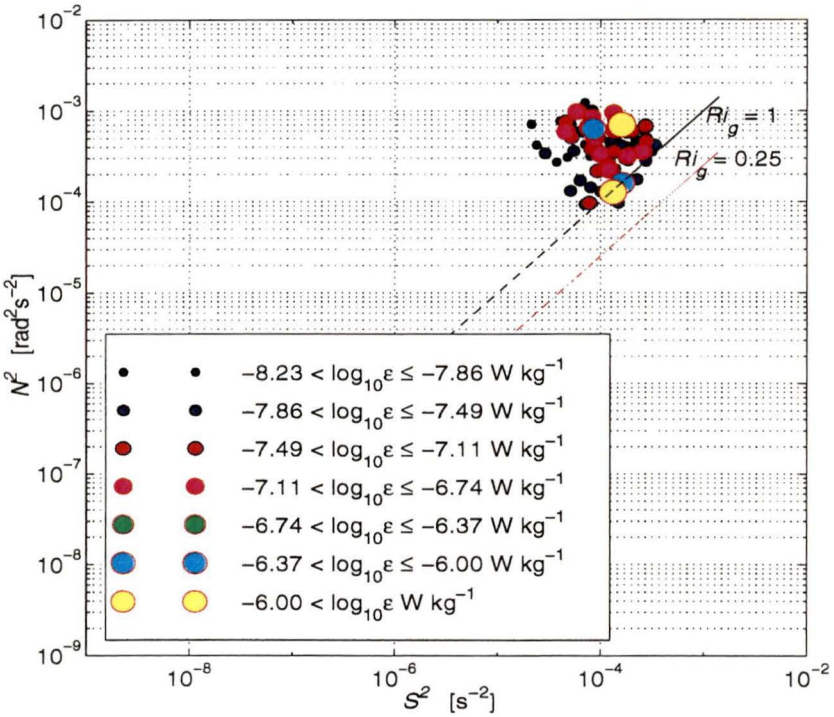

Figure 6.11: Shear, stratification and dissipation, tow 2. Larger circles indicate higher levels of dissipation.

buoyancy Reynolds' numbers, $Re_b < 15$ indicative that the turbulence had been suppressed and become wave-like in nature. Comparison was also made between the Ozmidov scale, L_O, and the Kolmogorov scale, L_K. It can be seen in figure 6.12 that L_O was frequently close to, or smaller than, the level of $(8.75 \pm 1.2)L_K$ which is equivalent to $Re_b = 18$.

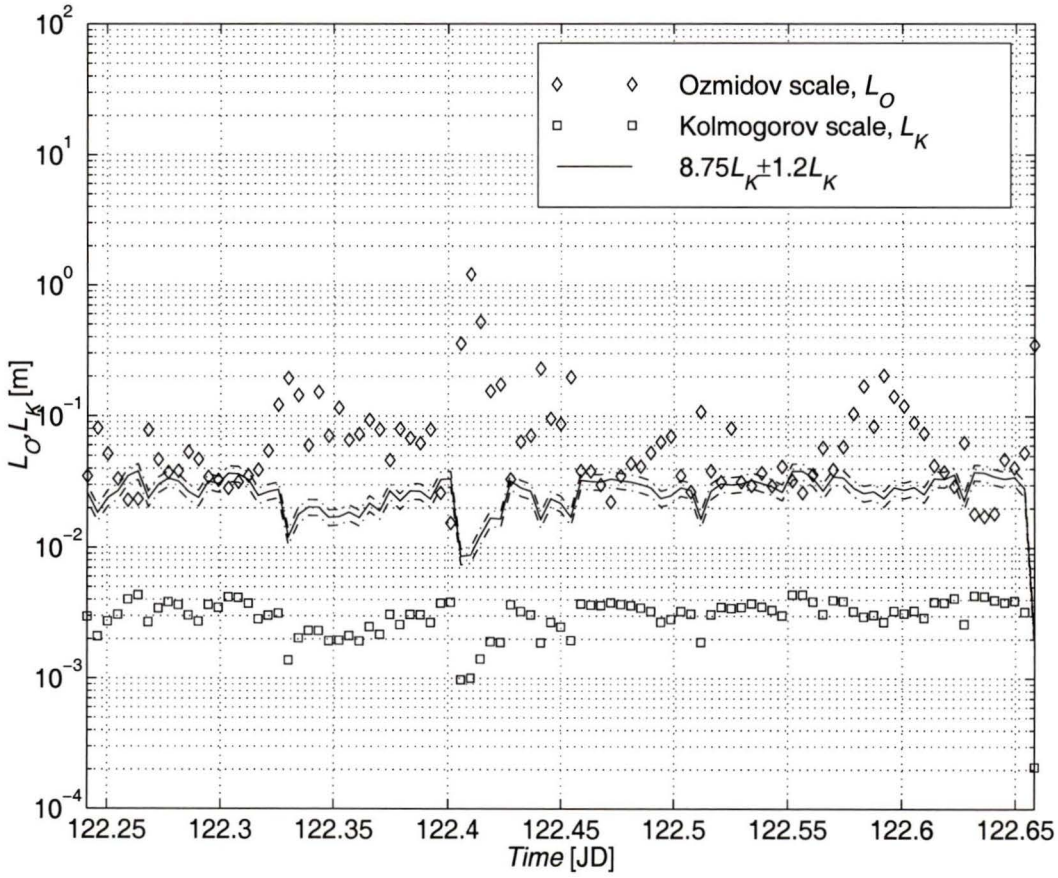

Figure 6.12: Ozmidov and Kolmogorov length scales, tow 2. The line at $8.75L_K$ is equivalent to $Re_b = 18$ and is the point at which Itsweire *et al.* (1986) found the turbulence to be suppressed and become wave-like in character.

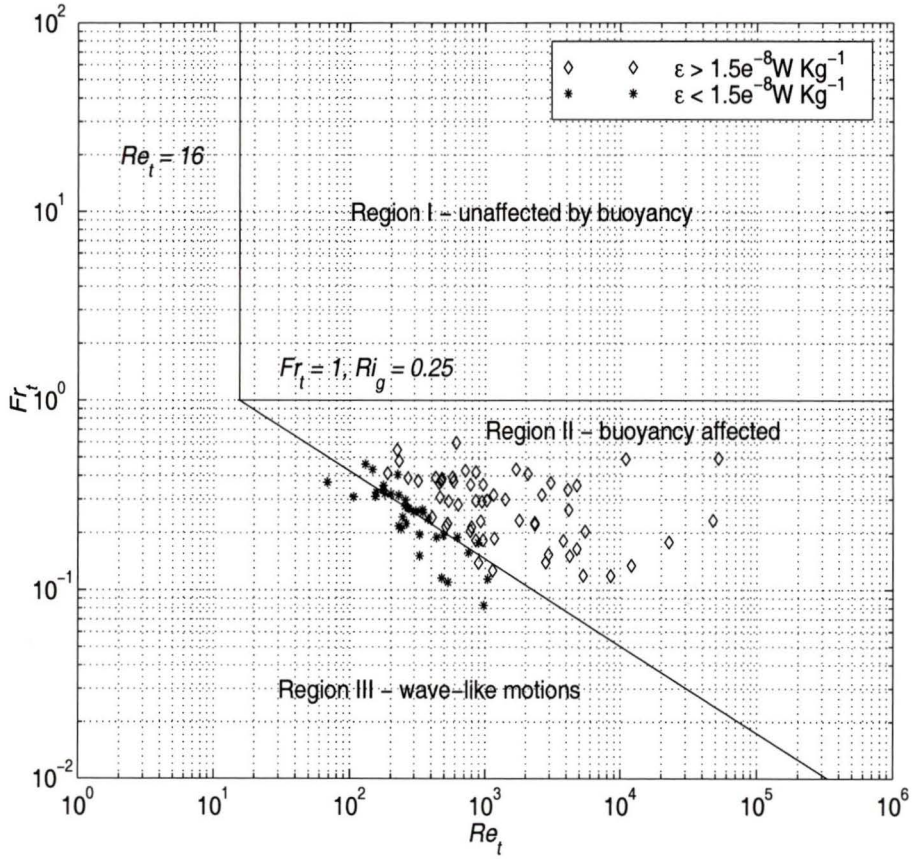

Figure 6.13: Turbulent Froude numbers and turbulent Reynolds' numbers, tow 2. The turbulence is heavily affected by buoyancy forces and some is suppressed. The line separating wave-like motions from turbulent overturns is equivalent to $Re_b = 16$.

6.3 Similarity scaling

Using the depth of *TOMI* and the Monin-Obukhov length, it is possible to classify the tow path into wind stress and buoyancy dominated regimes. Applying the appropriate dissipation scalings to the two tows it is seen that, with the exception of the period in tow 2 between JD122.33 and JD122.43 when the Monin-Obukhov length was very short, the scaling collapses the data at least as well as the results reported by Lombardo and Gregg (1989) or Shay and Gregg (1986) (i.e. within a factor of 2, figure 6.14).

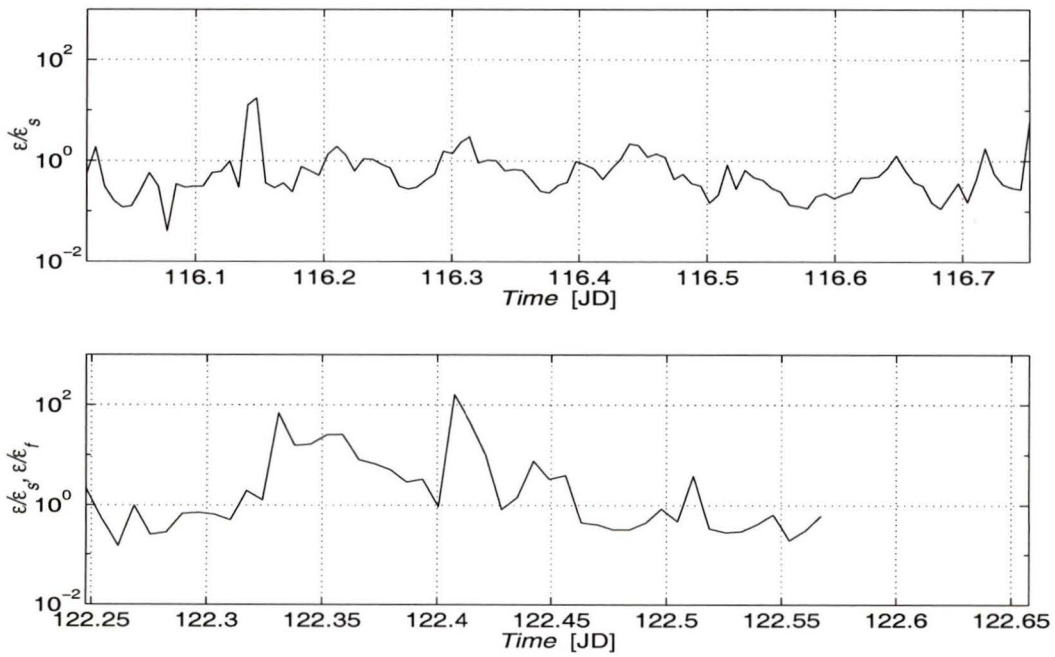

Figure 6.14: Measured dissipation normalized by similarity scaled dissipation (ϵ_s, ϵ_f) (a) tow 1 (b) tow 2.

This is particularly surprising for tow 1 in the light of the very different mechanism that appeared to be driving the instabilities. It is also interesting to note that where the similarity scaling failed worst in JD122, the wind stress was very low, the Monin-Obukov length very short (i.e. the dissipation should have been dominated by buoyancy forces) and this coincided with two bursts of temperature variance which did not appear to have associated low values of Ri_g.

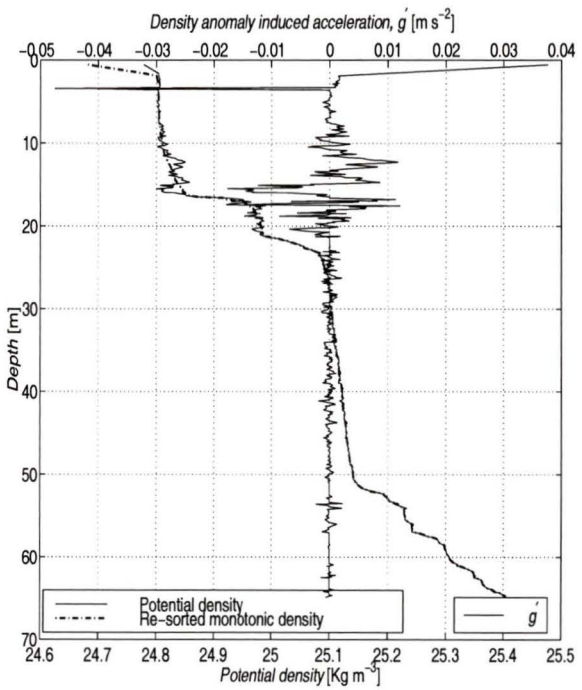

Figure 6.15: Potential density profile and density anomaly induced acceleration through shear layer, tow 1, JD116.24

A different scaling for shear driven turbulence at the base of the mixed layer was given by Sherman *et al.* (1978) who gave $\epsilon' = \Delta U g'_0$, where ΔU is the velocity difference across the layer. The mean "modified acceleration due to gravity" (Imberger

and Ivey 1991) across the interface, g'_0, was calculated by monotonizing the density profile using a bubble sort algorithm (Thorpe 1977) which was then subtracted from the original profile. The difference in density was then multiplied by g and divided by the mean density, ρ_0, to give g' at each point in the record of which the mean was taken.

From the CTD cast through the shear layer (Figure 6.15), $g'_0 = 7.22 \times 10^{-6}$ m s^{-2}, and taking the mean shear over the layer thickness of 7 m to be 0.018 s^{-1}, the estimate of $\epsilon' = 9.1 \times 10^{-7}$ W Kg^{-1} is also consistent with our measurements.

6.4 Log-normality of dissipation distribution

Two examples of turbulent shear and the associated dissipation distribution are shown in figures 6.16-6.17. In figure 6.16 the file mbl099 (JD116.243-116.262) from tow 1 is shown. This was measured by *TOMI* within the shear layer seen in the ADCP plots. The layer was very turbulent for the entire file and dissipation estimates were made spectrally from 2 second lengths of data. The comparison of the cumulative distributions for the measured and theoretical PDFs are shown in figure 6.16(c) and pass the Kolmogorov-Smirnov (KS) test at the 5% level.

Figure 6.17 shows a typical example of shear probe data from tow 2 (file mbl249, JD122.3445-122.3620). The turbulence was noticeably more intermittent and the associated dissipation distribution (figures 6.17(b-c)) failed the KS test at the 5%

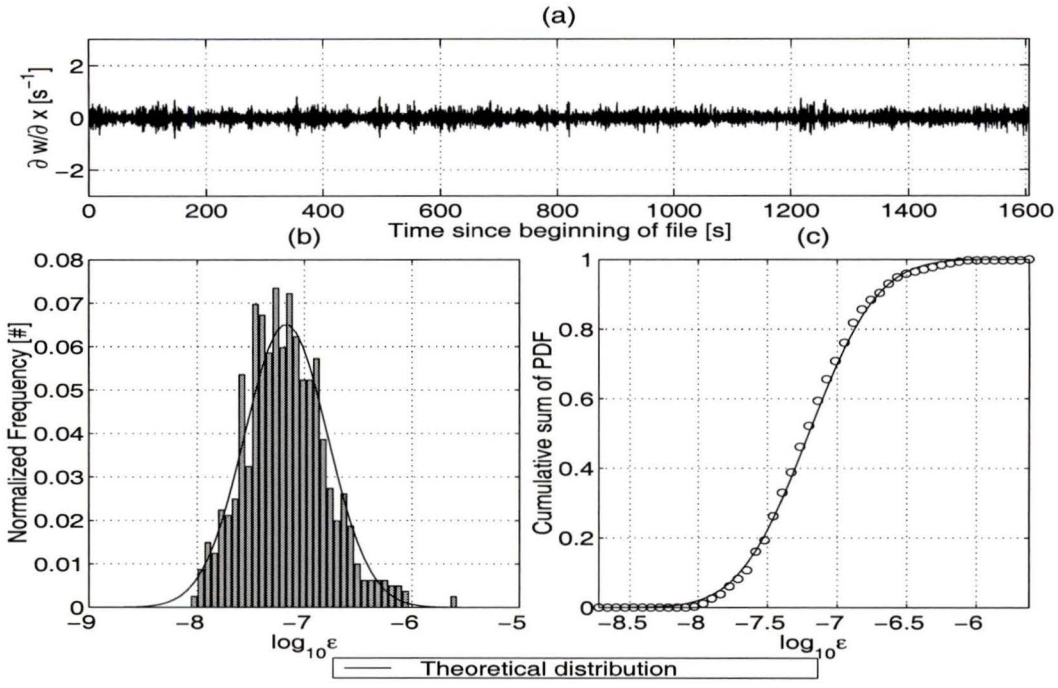

Figure 6.16: Data from tow 1 (file mbl099) (a) Sample of turbulence shear data (b) distribution of 2s dissipation estimates using the spectral method (c) cumulative distribution of measured distribution and theoretical estimate for a log-normal distribution.

level.

To test the hypothesis that the intermittency is the cause of the poor log-normal fit by the tow 2 data, a limited turbulent patch was selected (Figure 6.18(a), mbl249 660-670s) and compared with a limited very weakly turbulent patch (Figure 6.19(a) mbl268, 70-80s). Yamazaki and Lueck's (1990) point by point technique was employed on both sections of data after high pass filtering at 0.5 cpm with a single pole butterworth filter and low pass filtering at 100 cpm with a nine pole elliptic filter (0.3 db ripple in the pass band, 30 db in the stop band). This time-domain filtering

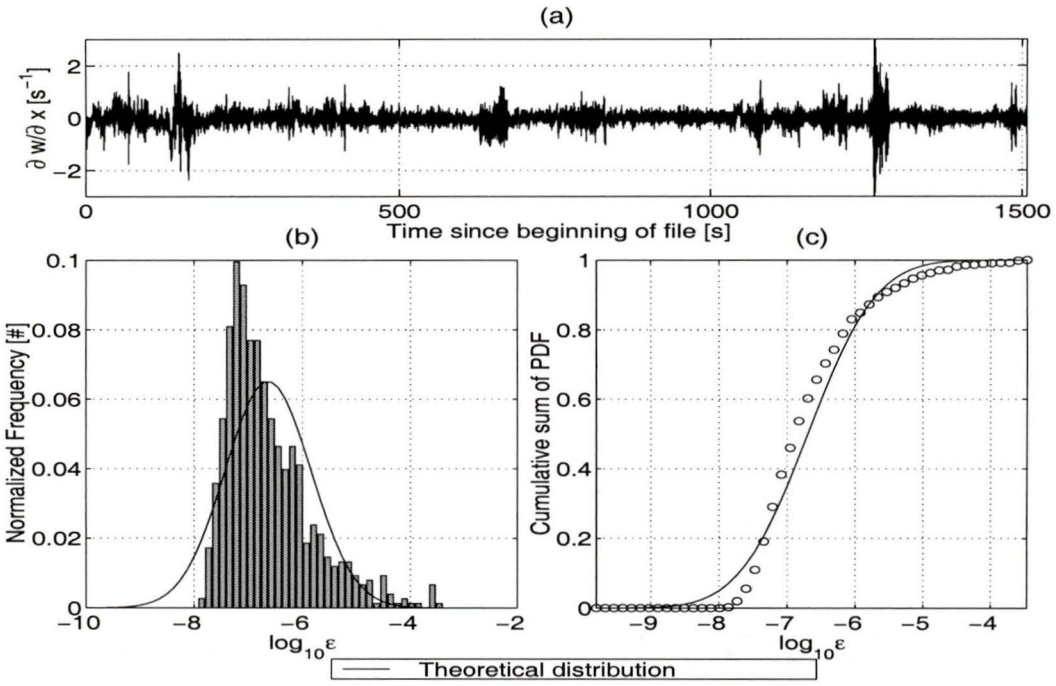

Figure 6.17: Data from tow 2 (file mbl249) (a) Sample of turbulence shear data (b) distribution of 2s dissipation estimates using the spectral method - note the poor fit to the log-normal curve (c) cumulative distribution of measured distribution and theoretical estimate for a log-normal distribution.

was performed in both the forward and reverse directions to preserve phase. The turbulent shear variance was averaged over 30 points and the distributions are shown in figure 6.18(b-c) and 6.19(b-c). In both cases, the use of data taken only from homogeneous patches produced distributions which passed the KS test at the 5% level. For the turbulent patch of mbl249, the mean dissipation rate was 1.00×10^{-6} W Kg^{-1} whilst for the particularly quiescent patch in mbl268, the dissipation rate was 1.25×10^{-8} W Kg^{-1}.

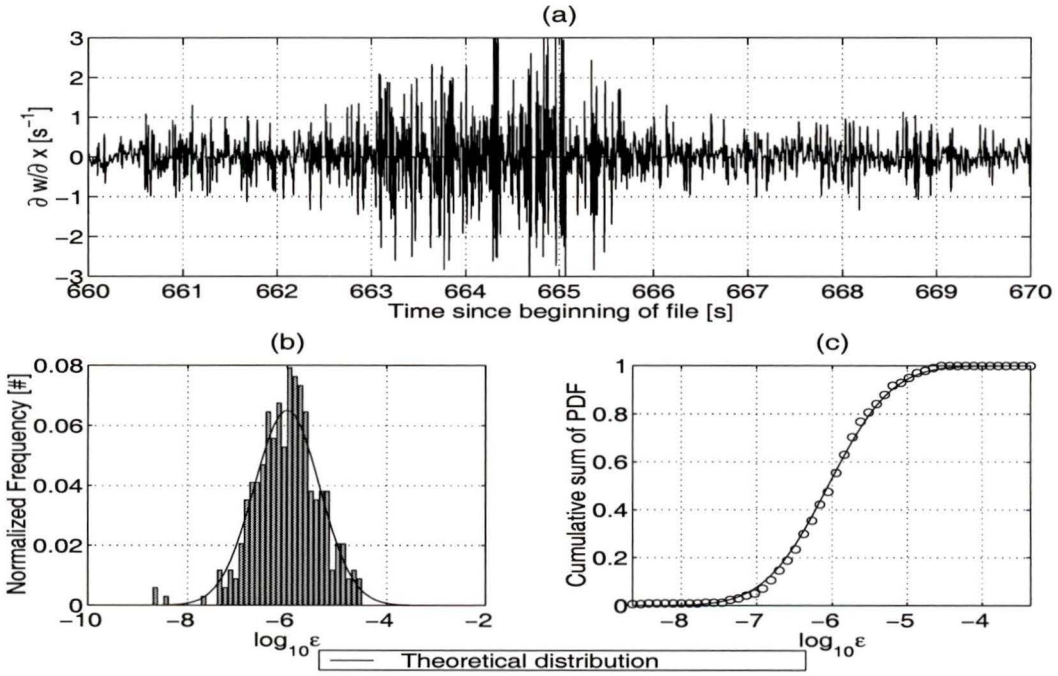

Figure 6.18: Data from mbl249 660-760s (a) turbulent shear data (b) distribution of dissipation estimates using the Yamazaki and Lueck (1990) point by point method (c) cumulative distribution of measured distribution and theoretical estimate for a log-normal distribution.

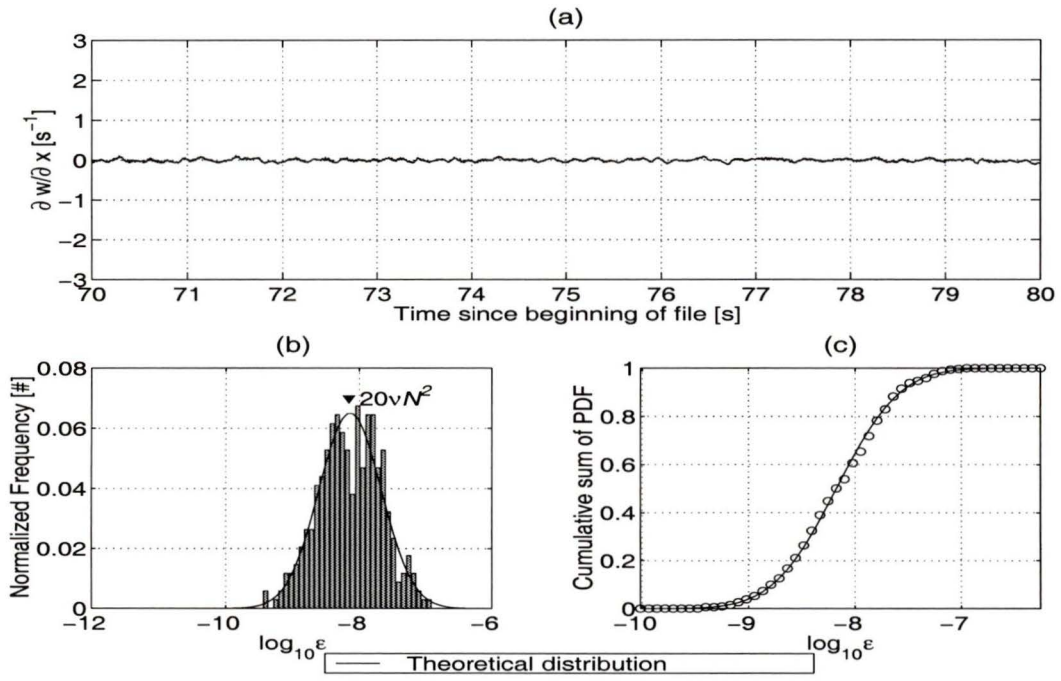

Figure 6.19: Data from mbl268 70-80s (a) turbulent shear data (b) distribution of dissipation estimates using the Yamazaki and Lueck (1990) point by point method (c) cumulative distribution of measured distribution and theoretical estimate for a log-normal distribution.

Chapter 7

Discussion

7.1 The macro-scale environment

The evolution of the ocean system through the duration of tow 1 is complex and difficult to explain. The time taken between leaving the warm layer at 36°25′ N, 122°19′ W and returning to the point in which warmer water had previously been encountered at 36°25′ N, 122°16′ W was approximately 50 minutes (Figure 4.2). However, the surface layer at this point appears to be 0.15°C cooler than it had been previously. At first sight, advection of the front to the south east would seem a plausible explanation. This is not likely for two reasons. Firstly, *DARSI*, the instrument that was being tracked and circled throughout this tow, is a drifting instrument with little windage. It is clear that on this basis the mean flow was to the south west, not to the south east. Secondly, the surface temperature pattern was repeated again as the ship moved south and is consistent with the advection of *DARSI* in a south westerly direction. On leaving the slightly warmer water, the ship moved into cooler water again at 36°22′ N, 122°20′ W and as the ship circled around, remained in cool water where warm water would again have been expected to be encountered.

Since the ship appeared to be able to go around this temperature feature, the only

consistent interpretation is that the patch of warm water was a "blob" which was being advected by the mean current and that our pattern of movement only touched the edges of it after initially crossing right through it. Without further observations, no more can really be said about the time evolution of the flow.

The complex evolution of the oceanic system on the time scale of tens of minutes raises the question of how best to sample under these conditions. Tow 2 was a deliberate effort to resample the area around the R/V *FLIP*. Even so, only one realization was achieved for most of the tow and the small portion that was resampled was only re-visited several hours after the first measurements were taken.

A better understanding of the nature of the fronts encountered in tow 1 and the associated mixing would have been greatly helped by a more cogent picture of what was happening at the larger scale. Several crossings of the front would certainly have been desirable along with "tow-yoed" CTD measurements to show the vertical density structure. Although the towed data from *TOMI* is very useful for understanding the horizontal structure of the ocean, vertical information is also very important. Mapping out the horizontal extent of the warm blob of water with CTD casts would also have helped. The use of differential GPS or even just the recording of the satellite information to allow post-processing of the ship's position would have enabled determination of absolute current velocities which were unavailable without bottom-tracking from the ADCP.

7.2 Shear generation by frontal dynamics

The close relationship of the shear layer, seen in the ADCP plots, with a step in density between two layers which were each quite homogeneous in both temperature and salinity, provides a strong argument in favour of the shear being generated by differential movement of the layers. The additional evidence of the shear layer sloping with depth, away from the surface, is also consistent with the model of re-stratification in which differential mixing produces density gradients which then relax with the lower density water moving over the denser water.

This picture of re-stratification (and the apparent thermal wind balance of the front, which produced shear of a magnitude very close to what is predicted for the horizontal density gradient seen in the front of tow 1) is very similar to that described by Tandon and Garrett (1994). The very important difference though is the lack of any detectable inertial signal in the shear record, which is predicted by Tandon and Garrett's solution. Tandon and Garrett also predict a peak gradient Richardson number of 0.5, which is larger than the $Ri_g < 0.25$ measured here.

It was noted in chapter 6 that inertial rotation of the velocity vector was apparent in the ADCP data prior to tow 1 but that there had been no rotation of the wind vector through the storm on JD108, which is a pre-requisite for the generation of inertial motions in the models of Gill (1984) and D'Asaro (1985). The re-stratification model of Tandon and Garrett may provide the source for the inertial motions observed. The

question is then why no inertial rotation was seen during tow 1.

The answer may lie in the time that had elapsed between the generation of the density gradients and the measurements made with the ADCP during tow 1. D'Asaro (1985) found that the best simulations of inertial forcing required that the damping constant for the inertial energy generated by a storm to leave the mixed layer was in the range of 2-10 days. Gill (1984) gives the time for the contribution of mixed layer energy to drop to $1/e$ of the total inertial energy as approximately 10 days. Gregg (1987) calculated the dissipation timescale of an inertial wave observed in the thermocline to be 4-8 days. If the density gradients were generated by the storm on JD108 then it is possible that a combination of dissipation and propagation of energy out of the mixed layer meant that inertial oscillations were not detectable by JD116 and that the density structure had relaxed close to geostrophic balance by that point. However, it is also likely that ageostrophic components to the flow also remained which produced values of Ri_g lower than Tandon and Garrett's (1994) predicted Richardson number.

7.3 Evidence for the process involved in the dissipation of shear layers

The evaluation of gradient Richardson numbers over an interval as short as 5 minutes is the significant achievement of this study. Oceanographic measurements of Richardson numbers have required averaging over much longer periods or have had

large possible errors associated with the shear. For example in Gregg *et al.* (1986), the use of 10 m shear obtained from their eXpendable Current Profiler (XCP) had significant errors associated with the lack of a pressure record to accurately juxtapose buoyancy frequency and shear. As a result, no correlation could be found between low Richardson numbers and dissipation in the persistent shear layer that they were observing. Hebert *et al.* (1991) had to calculate average Richardson numbers over 1 hour for the equatorial under-current (EUC). Large bin sizes on the ADCP and lower ping rates contributed to the uncertainty in the shear in this case. Vertical profiles of N^2 were only available at 10 minute intervals and this also led to the long averaging period.

The magnitude of the shear in the layer observed in tow 1 was large, comparable with that of the EUC (Peters *et al.* 1988). This large shear gives confidence that the noise level of the ADCP data was much lower than the measured signal.

The use of 5 minute averages of shear and stratification in association with dissipation estimates from the towed vehicle helps to present a coherent picture of shear driven mixing associated with low Richardson numbers. High shear regions visually coincide with high rates of dissipation and Richardson numbers below the theoretical critical value of $Ri_g = 0.25$. The visual relationship between the dissipation, shear and the stratification is also interesting. Simpson *et al.* (1990) observed the relationship between stratification and shear in estuarine flow. The shear has the effect

of both increasing the stratification and also providing the mechanism with which it can be eroded. The shear increases the stratification by constantly moving fluid mixed to a different density elsewhere in the flow (surface freshwater input in the case of Simpson *et al.*) into the active region. At the same time as this replenishment of stratified fluid is going on, the mean shear provides the energy for instabilities to grow and break down the stratification. If the flow was purely geostrophic then the shear could not induce stratification as the flow would no longer be re-stratifying. Any ageostrophic components to the shear could play a role in inducing stratification however. It has also been pointed out (R. Dewey, personal communication, 1998) that high shear can only persist in regions of high stratification, as in low stratification the gradient Richardson number would be very small and the momentum would quickly be mixed away.

This dual role of the shear may have important implications for phytoplankton. The echo intensity plots show a correlation with the shear layer. Osborn (personal communication, 1998) suggests that this correlation arises from the straining of patches of biology by the shear. Measurements of these layers show them to be very thin ($O(10^{-2} - 10^{0}$ m)) (Rines *et al.* 1999) and made up of colonies of diatoms formed in chains. Recent research by Rines *et al.* has shown that turbulence can break up these chains and has also suggested that thin layers of phytoplankton may be important for understanding the composition and succession of these communities.

There is sufficient variability in the measurements to mask any statistically significant correlation between either shear and dissipation or the gradient Richardson number and dissipation. The reason for this is likely to be that there is more than one mechanism involved in creating turbulence. It is noteworthy that although high dissipation occurs without low Richardson numbers, low values of Ri_g are always associated with large dissipation estimates. This suggests that instabilities may arise from internal wave breakdown and that shear on scales smaller than can be resolved by the ADCP can generate turbulence.

Although the critical value of Ri_g necessary for the onset of turbulence cannot be verified from these measurements, shear instability in the turbulent layer is clearly the dominant mechanism for breakdown. This being the case, the skewness of the temperature derivative was expected to follow the sign convention of Gibson *et al.* (1977). The lack of any relationship there is disappointing. Here however, the problem of averaging scale is most likely to be the reason for non-compliance. The scale of the temperature ramps presented by Thorpe and Hall (1980) was around 200-300m. At 1.25 ms^{-1} (a typical tow speed) this requires 4 minutes of tow per realization. Most of Thorpe and Hall's skewness measurements were averages of around 40 minutes towing in a single direction without the complication of fronts. The tow pattern of *TOMI* makes it clear that the ship's direction relative to the shear was changing constantly, meaning that more than one realization of any feature would be impossible, even

without the very obvious spatial variations in the flow and changes in tow depth. Tow 2 provided the straight tows which would be ideal for examining temperature skewness but the high stratification apparently suppressed any Kelvin-Helmholtz type billows and there was no visual indication of temperature ramps in the temperature record.

7.4 Statistics of TKE dissipation under different stratification regimes

Another significant finding of this work is that the shear layer in tow 1 was sufficiently turbulent to be considered statistically homogeneous with respect to dissipation. The close approximation to the theoretical log-normal curve sits in contrast to the highly intermittent nature of turbulence encountered in tow 2 where Richardson numbers were consistently large and stratification appeared to suppress the generation of turbulence. The ability to treat whole files as statistically homogeneous is extremely valuable when calculating flux Richardson numbers as will be seen below.

The comparison between the two tows, and the log-normality of isolated patches when approached with the Yamazaki and Lueck (1990) technique, shows that stratification has a big role to play in affecting the distribution of dissipation estimates. As further evidence of this, during file mbl119 (tow 1, JD116.585-116.604) when the ocean surface layer was convective, the 2 s spectral estimates were also found to be log-normal in their distribution, with a mean dissipation rate of 1.32×10^{-7} W Kg^{-1}.

Taking the two tows of JD116 and JD122 collectively, and classifying the slightly more statistically reliable 8 s spectral estimates by stratification, an interesting trend can be seen (Figure 7.1). Convective and neutral stratification regimes are found to be approximately log-normal (none actually pass the K-S test since the samples are not drawn from the same patch). As seen in table 7.1, for low stratification ($7 \times 10^{-6} < N^2 < 7 \times 10^{-5}$), the distribution is negatively skewed with high dissipation rates dominating, and a "tail" of low dissipation estimates, suggesting that weak overturns occur more frequently than a log-normal distribution would predict because of suppression by the stratification. Higher stratification causes the distribution to become progressively more positively skewed as energetic overturns become less frequent and the distribution becomes dominated by weak overturning events.

Stratification	**Skewness**
Convective ($N^2 < 0$)	-1.26±0.82
Neutral	
($-2 \times 10^{-6} < N^2 < 2 \times 10^{-6}$)	-1.01±0.75
$2 \times 10^{-6} < N^2 < 7 \times 10^{-6}$	-0.99±0.52
$7 \times 10^{-6} < N^2 < 2 \times 10^{-5}$	-1.40±0.33
$2 \times 10^{-5} < N^2 < 7 \times 10^{-5}$	-0.58±0.67
$7 \times 10^{-5} < N^2 < 2 \times 10^{-4}$	-0.46±0.18
$2 \times 10^{-4} < N^2 < 7 \times 10^{-4}$	1.34±0.18
$N^2 > 7 \times 10^{-4}$	2.77±1.04

Table 7.1: Skewness of dissipation distributions grouped by stratification. 95% confidence limits were calculated by the bootstrap method.

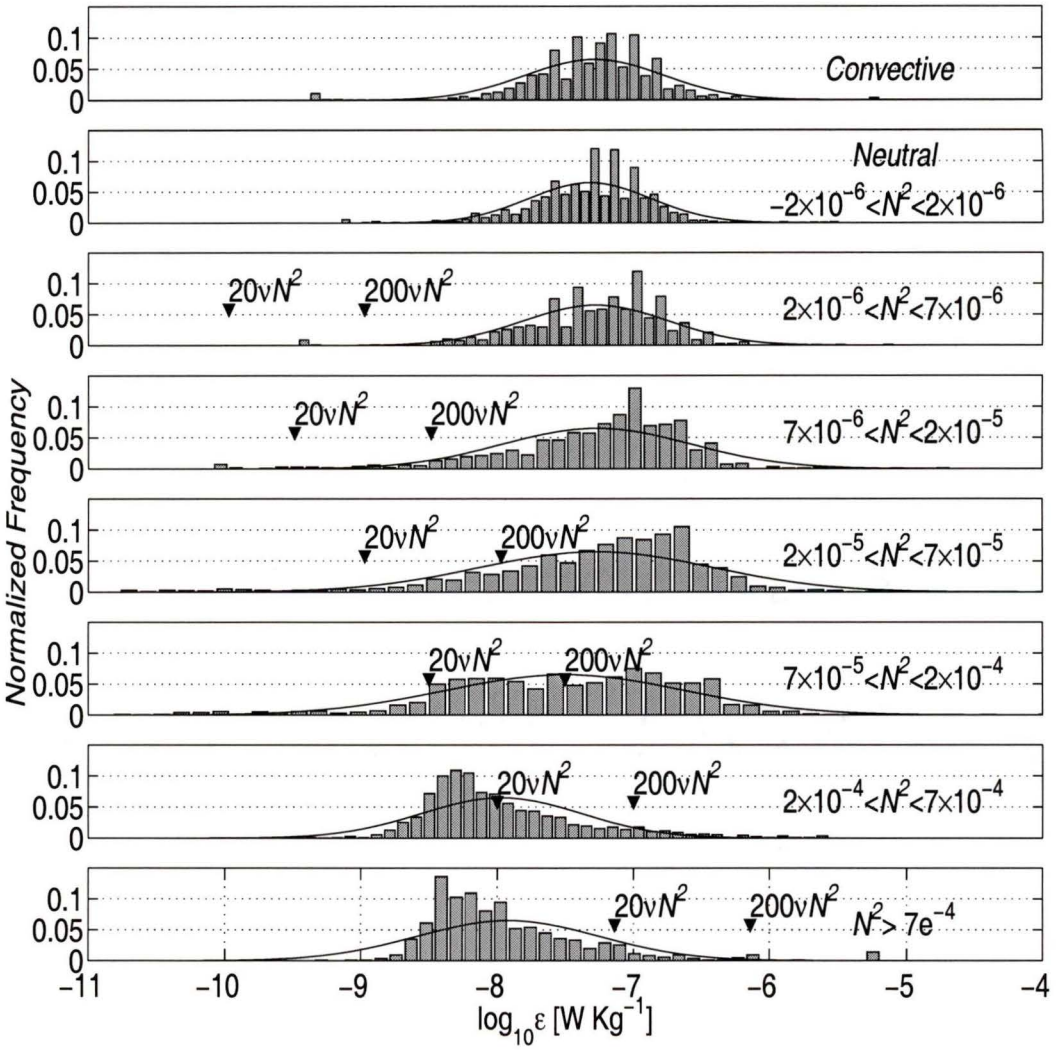

Figure 7.1: Dissipation distribution from tows 1 and 2 based on 8 s spectral estimates and grouped by stratification. Due to the high stratification of tow 2, the convective and neutral conditions in the top two plots are derived entirely from tow 1. The level at which buoyancy effects cause appreciable anisotropy in the inertial subrange is $\epsilon = 200\nu N^2$ and the level at which dissipation is suppressed is $\epsilon_{tr} = 20\nu N^2$.

This picture of suppression is consistent with the mixture of dissipation distributions presented in Yamazaki *et al.* (1990). In that paper it was hypothesized that the two elements of the bi-modal distribution represented an "active" and a "quiescent" mode. How can such bimodality, rather than a continuum distribution, be produced under these circumstances? A similar bimodality is found in the data presented here (Figure 7.2). It is suggested that the answer lies in the observed catastrophic collapse in buoyancy production at the point where turbulence is suppressed (discussed below in section 7.5) which also has a concurrent collapse in the dissipation rate. Yamazaki

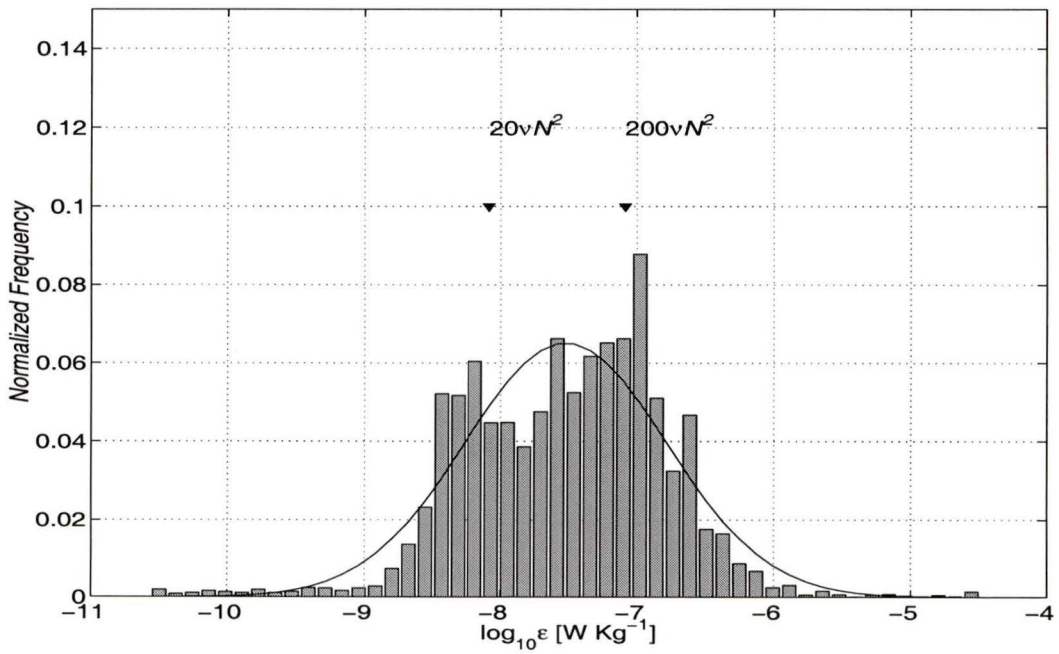

Figure 7.2: Dissipation distribution from tow 1 and tow 2 based on 8 s spectral estimates. The level at which buoyancy effects cause appreciable anisotropy is $\epsilon = 200\nu N^2$ and the level at which dissipation is suppressed is $\epsilon_{tr} = 20\nu N^2$.

et al. found that the lower mode consisted of suppressed turbulence, below the transition dissipation rate of $\epsilon_{tr} \approx 20\nu N^2$, at which point the turbulence becomes wave-like in nature. This suggests that there is an evolution of the form of the dissipation distribution from "active" low gradient Richardson number turbulence through "buoyancy affected" turbulence and then a sudden collapse to suppressed turbulence. Figure 7.2 shows that the lower mode observed here is also consists of suppressed turbulence.

The distribution of the wave-like turbulence is uncertain. The very quiescent section of data from file mbl268 shown in figure 6.19 is from a section for which Re_b falls below the transition value for part of the distribution. However, the distribution is still very log-normal. In figure 7.1 the highest level of stratification has a distribution for which all the dissipation estimates are below the transition dissipation rate. The distribution looks to be approaching a normal distribution rather than log-normal. The rate of viscous dissipation of this suppressed turbulence is still quite high compared to expected instrumental noise levels, though the use of isotropic relations is clearly inapplicable here. Estimates as low as 5×10^{-10} W Kg^{-1} are shown in figure 7.2 setting this as the estimated cut-off for instrumental noise. The normal distribution of the wave-like turbulence may therefore suggest that this represents background oceanic "noise", rather than instrumental noise.

Lueck *et al.* (1997) had a similar result in the very quiescent waters of Satellite Narrows where, despite very short Ozmidov scales and about half of their buoyancy

Reynolds' numbers falling below the transition value, dissipation spectra in close agreement with the universal spectrum were still obtained.

7.5 Flux Richardson numbers in active and decaying turbulence

Perhaps one of the most interesting questions posed by direct oceanographic measurements of Rf (e.g. Gargett and Moum 1995, Wolk 1997), is why they can apparently exceed the critical values obtained from theoretical arguments and laboratory experiments (Table 7.2). Much scepticism has surrounded direct ocean measurements because of the difficulties in removing body motions from the signal of the vertical component of turbulent fluctuations. Even after highly sophisticated methods of motion correction have been employed, such as those used by Wolk (1997), the size of the correction means that long averaging periods need to be adopted to ensure the statistical reliability of the results. Such long averaging poses questions about how well the assumption of statistical homogeneity is complied with. Here it has been shown that the assumption holds extremely well when the Richardson number is low for long periods in an environment which has a constant energy source, such as the shear layer or the convective regime in tow 1.

The problem is this: We have a stably stratified shear flow for which both theory and laboratory observations suggest there should be a critical flux Richardson number, Rf_{crit}, above which turbulence cannot be sustained because too much energy is

Theory	Rf_{crit}
Ellison (1957)	0.15
Townsend (1958)	0.50
Thorpe (1973a)	0.29
Laboratory Experiments	Rf
Ellison and Turner (1960)	0.05-0.35
Thorpe (1973b)	0.21-0.27
Stillinger *et al.* (1983)	0.01-0.15
Itsweire *et al.* (1986)	0.01-0.24
Oceanographic Measurements	Rf
Taylor (1931)	0.3
Woods and Wiley (1972)	0.32
Gargett and Moum (1995)	0.41
Moum (1996)	0.13-0.17
Wolk (1997)	0.29-0.35

Table 7.2: Comparison of flux Richardson number estimates

required to do work on the stratification. Theoretical arguments and observations both suggest that this number is much less than 1. But how much less than 1? The difference in the estimate of K_ρ using Osborn's (1980) method between assuming $Rf = 0.15$ and taking $Rf = 0.4$ is nearly a factor of 4.

The accepted hypothesis for the partitioning of energy in turbulent eddies is that stratification removes energy only from the vertical component of the turbulent fluctuations (2.16), and that energy from the mean shear goes first into the u component (2.14) from where it is distributed to v and w by pressure fluctuations (which is assumed to be an inefficient process since isotropy requires an energetic flow). At some point, the loss to stratification is too great to sustain vertical overturning motions. Stewart's (1959) argument assumed that pressure re-distribution from u into v and w is equal. If this apportionment remains fixed and stratification is acting upon the overturn then v must have more kinetic energy than w. Laboratory experiments by Stillinger *et al.* (1983) and Itsweire *et al.* (1986) show that u is consistently more energetic than w in stratified fluids although measurements of v were not reported. The complete transition to a wave-like state in these experiments is considered to have occurred where $\overline{\rho w} = 0$, as proposed by Stewart (1969).

Ivey and Imberger (1991) showed (using data from Itsweire *et al.* (1986)) that the flux Richardson number peaks at $Rf \approx 0.2$, at a turbulent Froude number, $Fr_t = 1$ ($Ri_g = 0.25$). Ivey and Imberger suggested that Rf is only dependent on Fr_t and

independent of the turbulent Reynolds' number, Re_t, and so assumed scalability to the larger turbulent Reynolds' numbers of the natural environment. However, there are TWO independent scales affecting the flux Richardson number and Rf is NOT independent of the buoyancy Reynolds' number, Re_b (Figure 7.3).

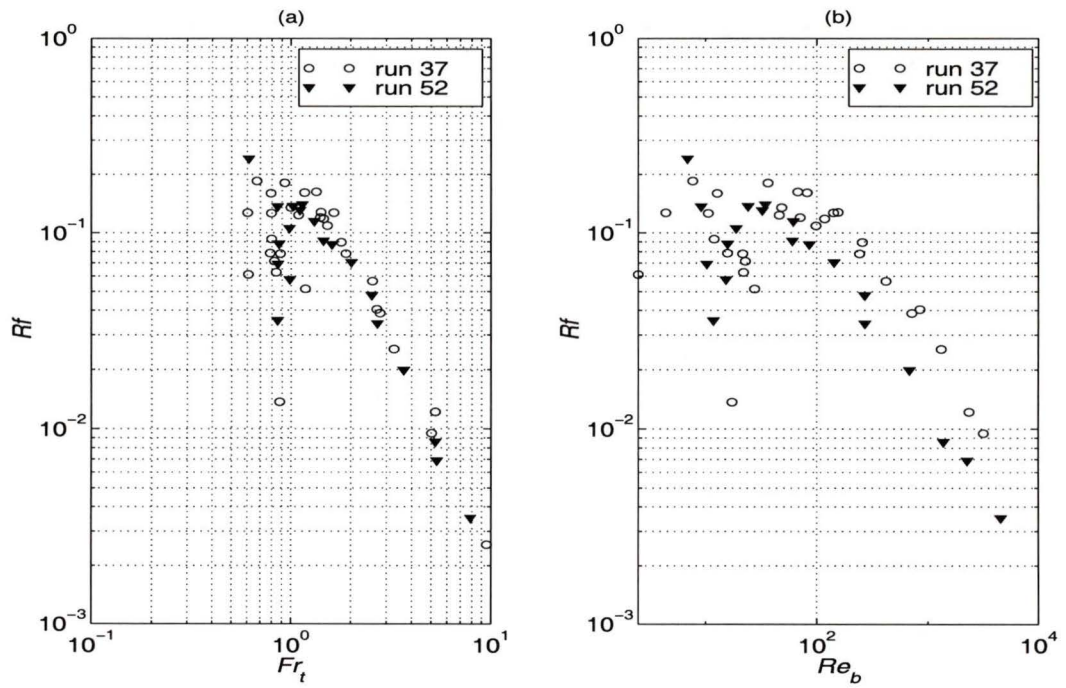

Figure 7.3: Relationship between laboratory measurements of (a) turbulent Froude number and flux Richardson number (b) buoyancy Reynolds' number and flux Richardson number. Data has been taken from Itsweire *et al.* (1986).

As discussed above, previous work has shown that turbulent motions cease and become wave-like in nature when $Re_b \approx 20$ (Stillinger *et al.* 1983), and are strongly affected by stratification for $Re_b < 200$ (Gargett *et al.* 1984). The peak value of $Rf = 0.2$ not only coincides with $Fr_t = 1$ ($Ri_g = 0.25$) but also with $Re_b \approx 20$ and

drops exponentially for larger values of Re_b. The relationship of Rf with Ri_g fits well with the scaling arguments of Garrett (personal communication, 1998). If ϵ scales as u^3/l and K_v scales as ul then for $Ri_g << 0.25$ with density acting as a passive scalar we can write

$$\begin{aligned} \frac{Rf}{1-Rf} &= \frac{K_v N^2}{\epsilon} \\ &\approx \frac{ulN^2}{u^3 l^{-1}} \\ &\approx \frac{N^2 l^2}{u^2} \\ &\approx \frac{N^2}{S^2} = Ri_g \end{aligned} \tag{7.1}$$

It can be seen in figure 7.3(a), that the slope falls off 2 decades in Rf against 1 decade in Fr_t, which implies $Rf \propto (S/N)^{-2}$ and hence $Rf \propto Ri_g$. Below the critical value of Re_b we see the sort of catastrophic collapse of Rf predicted by Townsend (1958). This is also consistent with the work of Ellison (1957) which estimated that at the transition point, the ratio of the eddy coefficient for heat to the eddy coefficient for momentum, $K_H/K_M = 0$ and $Rf = 0.15$. This collapse has already been suggested to result in the observed bi-modality of the dissipation distribution. To extrapolate the relationship of Rf and Re_b to our measurements in the ocean where the buoyancy Reynolds' numbers are O(10^4) we have values of $Rf \approx 0.01$, which is significantly different from the direct measurements of Wolk (1997), Fleury and Lueck (1994) or Gargett and Moum (1995). How can we reconcile the apparent contradiction that $Rf \rightarrow 0$ for large Re_b and yet measure $Rf > 0.3$?

Townsend (1958), Ellison (1957) and Stewart (1959) all approached the problem by assuming homogeneous, isotropic turbulence. As the transition point to the wave-like state is approached, this is obviously not the case and points towards an explanation of what is happening. The issue is that high Re_b implies a large separation between the energy containing and dissipative scales and the existence of isotropy over some range of the velocity spectrum. Under isotropic conditions, Stewart's (1959) reasoning shows that all components of the turbulence must have equal kinetic energy and so either there is no work being done against the stratification by these overturns ($Rf = 0$), or else the pressure forces must compensate for losses to buoyancy by preferentially distributing energy into the vertical component.

One of the problems with Ellison's (1957) arguments is that having assumed isotropy, he then took the case of $K_H/K_M = 0$ as the point at which turbulence is suppressed. This is quite inconsistent with the concept of isotropy. Moreover, in order to evaluate Rf_{crit}, Ellison assumed that the decay time scales for the density fluctuations and the velocity fluctuations are approximately equal which is inconsistent with $K_H/K_M = 0$. For these reasons, Ellison's value of $Rf_{crit} = 0.15$ should be treated with caution. On the other hand, Townsend (1958) assumed complete isotropy which, on the basis of the arguments set out above, is inconsistent with the requirement of anisotropy in order for work to be carried out on the stratification. Townsend's finding of $Ri_g < 1/12$ for a buoyancy flux to be maintained, was rather

smaller than experimental results have suggested, but nonetheless, the result does show $Rf \propto Ri_g$ as outlined above in equation 7.1.

Now, it is hard to imagine how the largest scales of motion, the energy containing scales, could be anything but *an*isotropic and doing work against the stratification. The vertical length scale of the largest overturns is given by the Ozmidov length. For tow 1, L_O has a mean of 7 m. The spectrum of the buoyancy flux peaks at 14 m (Wolk 1997) for the stratified case which, if we assume that this is also the horizontal scale of the most energetic eddies, implies an aspect ratio of 0.5. This aspect ratio is actually at the "rounder" end of the atmospheric observations by Browning (1971) who observed aspect ratios, η, of

$$0.097 < \eta < 0.500.$$

Whilst Ri_g is maintained below 0.25 the flow is unstable and instabilities continue to grow. Thorpe (1973b) reported that the entrainment velocity of the instabilities, which is the rate at which a turbulent layer erodes the interface of a stable layer, is given by $E \propto Ri_g^{-1}$. This implies that the low Richardson number regions of tow 1 were growing and continuing to entrain fluid. Overall, the shear layer was likely to be in approximately steady state, with instabilities both growing and decaying, since the shear layer was observed over several days prior to tow 1. The turbulent Froude number is inversely proportional to the gradient Richardson number and it may be recalled that a turbulent Froude number of 1 is equivalent to $Ri_g = 0.25$.

Figure 7.4 shows that Fr_t also scales with the buoyancy Reynolds number showing that large values of Fr_t and hence small values of Ri_g are associated with large buoyancy Reynolds' numbers. The displacement of the oceanographic data to lower turbulent Froude numbers than measured in the laboratory is indicative that not all the shear was resolved by the ADCP and that, as suggested in chapter 6, the gradient Richardson numbers are overestimated.

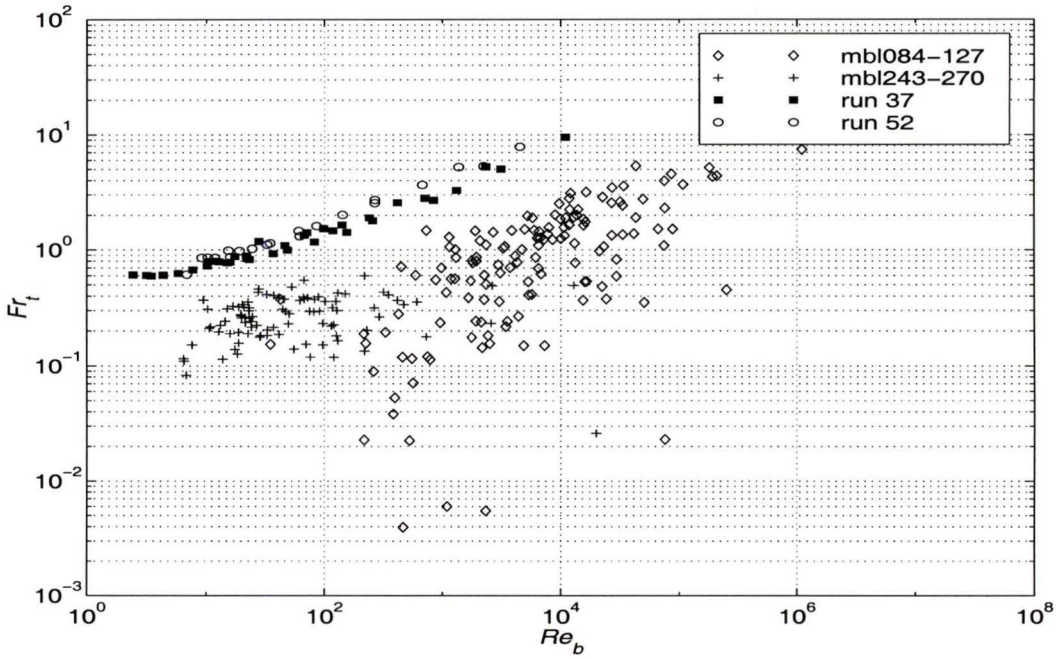

Figure 7.4: Relationship between laboratory measurements of buoyancy Reynolds' number and turbulent Froude number. Data has been taken from Itsweire *et al.* (1986) and compared with data from tow 1 (mbl084-127) and tow 2 (mbl243-270).

Both Gargett and Moum (1995) and Wolk (1997) have suggested that the large values of Rf they measured could be due to the input of energy directly into the

w component, resulting from vertical shear associated with fronts. Although frontal activity was certainly significant during tow 1, the scale of the fronts does not match well with the scales over which Wolk found the high flux Richardson numbers. Bubble penetration detected by the sonars also suggested that Langmuir cell penetration was too shallow to affect Wolk's measurements.

The development of the large scale overturns induced by shear has been shown by Thorpe (1973b) to be highly structured and essentially 2-dimensional, consisting of tube-like billows with crest lines orientated in the direction of the vorticity vector of the initial flow. Under these circumstances, there is no viscous loss to the v component and so energy partitioning is only between viscous losses from u and w and losses to buoyancy from w. It is suggested from this that the reason the laboratory measurements of Rf_{crit} are inconsistent with the oceanographic data is not because of energy derived from vertical shear but instead results from scale separation between the anisotropic energy containing eddies and the isotropic dissipation. The concept of a critical flux Richardson number applies very well to 3-dimensional turbulence in the transition to a wave-like state but the dissipative scales are irrelevant to the work being done against the stratification by the energy containing scales in a maintained shear flow. The partitioning of energy under these conditions appears to be essentially 2-dimensional and the anisotropy of the large scales which led to Wolk (1997) finding that the peak buoyancy flux occured at a wavelength of 14 m suggests that the vertical

measurements by Moum (1996) failed to resolve the buoyancy flux and hence Moum found lower flux Richardson numbers.

7.6 The applicability of similarity scaling

The apparent ability of similarity scaling to collapse the dissipations measured in tow 1 is intriguing given that the source of the instabilities appeared to be shear arising from the thermal wind balance of the two layers of water. Variability over 2 orders of magnitude is still apparent in tow 1 and so it is possible that the scaling is simply coincidental. Without vertical profiles of dissipation it is impossible to know whether the shear layer is anomalous to the scaling of the mixed layer as a whole.

The largest deviation from the similarity scaling occurred in tow 2 and was associated with a time of very low winds and low shear and Richardson number greater than 1 (Figure 6.10). A patch of strong temperature variance is correlated with this deviation and may be related to internal wave activity within this highly stratified layer.

Chapter 8

Summary, Conclusions and Further Work

8.1 Summary

Data have been presented which were collected by our instrument, *TOMI*, during two tows in very different conditions. In the first tow there was significant wind forcing and the mesoscale ocean surface temperature pattern was evolving on the time scale of tens of minutes. Stratification was generally weak with some convective areas. A strong shear layer was also detected which was associated with density fronts. In the second tow, the energy input to the surface layer from wind forcing was an order of magnitude lower and the ocean was highly stratified. No significant shear layers were detected.

The strong shear of the first tow coincided precisely with a large density gradient between two layers which were each nearly homogeneous in temperature and salinity. The shear layer sloped and reached the surface where the surface temperature pattern showed an abrupt change. The magnitude of the shear across the temperature front matched closely with the theoretical shear calculated from the thermal wind equation.

Gradient Richardson numbers calculated over 5 minute periods were frequently found to be below the theoretical critical value for the onset of turbulence, $Ri_{crit} = 0.25$, in the high shear layer of the first tow. Dissipation rates were correspondingly

higher in these low *Ri* regions. Stratification was also observed to be higher in the shear layer and regions of strong echo had a close correspondence with the shear layer, extending over O(10) Km.

The distribution of dissipation rates was found to be log-normal for the duration of a whole file in the turbulent shear layer and in a convective layer. Distributions taken from the highly stratified tow 2 were distinctly non-lognormal but point-by-point distributions of dissipation taken from a single patch did show log-normality as did short sections of data taken from extremely quiescent regions, even though the dissipation levels showed that the turbulence should have been suppressed and become wave-like in nature for part of the distribution.

Bi-modality of the dissipation distribution for the two tows combined was observed. The lower mode was found to be comprised of suppressed turbulence. Comparison of the distributions when categorized by stratification level showed a progression of the distribution from being essentially log-normal in form in neutral or convective conditions, through negative skewness of the distribution for low stratification to positive skewness for high stratification.

Similarity scaling appeared to normalize the dissipation data as well as had been previously reported (within two orders of magnitude) except for a period of low winds and high stratification during tow 2. Scaling of the dissipation with a parameterization applicable to shear at the base of the mixed layer normalized the dissipation

equally well for the data collected in the shear layer during tow 1.

Flux Richardson numbers calculated with parameterizations based upon the turbulent Froude number and buoyancy Reynolds' number disagreed badly with direct flux measurements.

8.2 Conclusions

I. *Shear*

(a) Intense shear may have been generated as the result of the re-stratification of two layers which may have been unequally mixed in a storm 8 days prior to the measurements made in tow 1.

(b) The magnitude of the shear was well explained by the thermal wind equation which suggests that the density front was no longer re-stratifying and was close to geostrophic balance. The lack of any inertial shear signal from the re-stratification process, which was predicted by the model of Tandon and Garrett (1994), suggests that the inertial energy had already radiated away from the area as the two layers came into geostrophic balance. This could explain the observations of inertial rotation of the shear vector in the days following the storm and prior to the first tow, despite the lack of rotation of the wind vector during the storm.

(c) Gradient Richardson numbers smaller than predicted by Tandon and Garrett may have been generated by ageostrophic components of the shear.

(d) Ageostrophic components of the shear may play a role in inducing the stratification (and also provide the energy to break it down) by moving fresh fluid into the mixing region. At the same time, straining of patches of phytoplankton, identified as areas of high echo intensity, may have significant implications for the evolution of the flora within the patch.

II. *Richardson numbers, temperature variance and dissipation*

(a) Gradient Richardson numbers below the theoretical critical value of $Ri_g = 0.25$ relate closely to enhanced rates of dissipation. Dissipation rates are always high when Richardson numbers are low but some high dissipation rates occurred when Richardson numbers were above the critical level. The dissipation not occurring at low Richardson numbers is thought to derive from internal wave breaking and shear at scales unresolved by the ADCP.

(b) High rates of dissipation are always associated with patches of temperature microstructure but the converse is not always true, possibly suggesting the "footprints" of past turbulent events.

(c) The eddy coefficient for density, K_ρ, is not elevated in the front and is actually smaller in the high shear/high dissipation regions than outside them, due to the concurrent increase in stratification in the shear layer.

(d) Despite the evidence for shear induced turbulence in tow 1, temperature gradient skewnesses were not found to match the sign convention of Gibson *et al.* (1977). This mismatch is attributed to the rapid variation in ship direction in comparison with the scale of the expected temperature ramps and the frontal activity encountered.

III. *Similarity scaling*

(a) Similarity scaling appears to normalize the data despite significant evidence that the forcing mechanism is related to the re-stratification mechanism and not to surface buoyancy forcing or wind stress. The normalization of the data by similarity scaling is as good as that reported by Lombardo and Gregg (1989) except for a period characterized by low winds, low shear and high stratification during which a patch of intense temperature microstructure was observed. This dissipation and temperature microstructure is conjectured to have resulted from internal wave breaking.

IV. *Dissipation distribution*

(a) Bi-modality of the dissipation distribution is attributed to the collapse of dissipation levels and buoyancy fluxes at the transition point from turbulence into a suppressed wave-like state. This collapse is predicted by theory and laboratory measurement to occur at $Ri_g = 0.25$ but this is

unable to be substantiated from the present measurements. However, the bi-modality does fit well with the laboratory finding that suppression occurs at a buoyancy Reynolds' number, $Re_b = 20$.

(b) Dissipation distributions can be log-normal without being from the same patch if the turbulence is intense enough that the turbulent layer can be considered homogeneous. Log-normality of dissipation estimates is found to occur within single patches occurring in highly stratified and intermittently turbulent environments.

(c) The distribution of wave-like turbulence which has dissipation rates higher than estimated instrumental noise levels, seems to approach normal, suggesting that this represents background oceanic "noise".

V. *Flux Richardson numbers*

(a) The prediction by laboratory measurements of very low flux Richardson numbers for the high buoyancy Reynolds' number flows observed in the first tow is contradicted by direct measurements.

(b) A large separation between the energy containing scales and the dissipative scales implies that the dissipative scales are isotropic. It is suggested that the discrepancy between the laboratory measurements and the direct oceanographic flux measurements arises from this scale separation and that the anisotropic energy containing scales are essentially 2-dimensional

whereas the isotropic dissipative scales are 3-dimensional.

8.3 Further work

The relationship of the flux Richardson number to the anisotropy of the energy containing scales and the hypothesized 2-dimensionality of those scales is a subject which should be investigated. Along with this, verification of the sign of the temperature gradient skewness in maintained, free shear flows and a clearer understanding of the relationship of the gradient Richardson number to the rate of dissipation and buoyancy production should be sought.

A suitable experiment would be conducted in a highly stratified environment which is subject to predictable forcing, such as a tidally dominated estuary. The channel would ideally be fairly straight and be free from major bed topography which might complicate the turbulence generation mechanism, and the forcing should provide high Reynolds' number shear generated turbulence for a sustained period. The depth should ideally be within the range of bottom-tracking by an ADCP, but deep enough that bed generated turbulence does not interfere with the free shear flow. In addition, frontal activity should be avoided if at all possible. Straight tows in directions with and opposed to the mean current as well as perpendicular to the mean current would be made with *TOMI* to identify coherent structures and their form. Ideally these tows should be carried out at varying stages of the tidal cycle and repeated over a

number of tidal cycles. This would allow measurements of turbulence with different Reynolds' numbers and also allow differences between growth and decay cycles to be identified. *TOMI* would be used for both single depth tows and in profiling mode to gain additional information on the vertical structure of the turbulence. The motion correction procedure of Wolk (1997) would be used to allow direct calculation of flux Richardson numbers. Vertical profiles of temperature and salinity would be collected by a "tow-yoed" CTD.

Additional to the usual suite of temperature and salinity sensors, shear probes and body motion sensors, *TOMI* would be equipped with *SONAR* optimized for the detection of Kelvin-Helmholtz type instabilities. The ship would be equipped with a broad-band, bottom-tracking ADCP, have real-time differential GPS or record GPS satellite information to allow post-cruise processing. The ADCP should have a high ping rate and be set to average pings over as small a volume as possible. Such a set-up would permit accurate measurement of absolute current velocities and allow gradient Richardson numbers to be calculated with better resolution of the shear than has been previously possible. A towed 2-dimensional array of thermistors would provide further information about the 3-dimensionality of coherent structures and allow the associated temperature gradient skewness to be calculated. Further information could be gained from the use of high resolution vertical current profilers which would allow an assessment of the loss of shear variance in the ADCP measurements. Standard

meterological measurements would also be collected to allow the calculation of bulk surface forcing parameters.

Laboratory experiments focussing on the dissipation within suppressed, wave-like "turbulence" should be conducted to provide insight into this unresolved issue.

References

Anis, A., and J. Moum, The superadiabatic surface layer of the ocean during convection., *Journal of Physical Oceanography*, *22*(10), 1221–1227, 1992.

Antonia, R., A. Chambers, C. Friehe, and C. van Atta, Temperature ramps in the atmospheric surface layer., *Journal of the Atmospheric Sciences*, *36*, 99–108, 1979.

Browning, K., Structure of the atmosphere in the vicinity of large amplitude Kelvin-Helmholtz billows., *Quarterly Journal of the Royal Meteorological Society.*, *97*, 283–299, 1971.

Chereskin, T., D. Halpern, and L. Regier, Comparison of shipboard Acoustic Doppler Current Profiler and moored current measurements in the equatorial Pacific., *Journal of Atmospheric and Oceanic Technology*, *4*(4), 742–747, 1987.

D'Asaro, E., The energy flux from the wind to near-inertial motions in the surface mixed layer., *Journal of Physical Oceanography*, *15*(8), 1043–1059, 1985.

Edson, J., A. Hinton, K. Prada, J. Hare, and C. Fairall, Direct covariance flux estimates from mobile platforms at sea., *Journal of Atmospheric and Oceanic Technology*, *15*(2), 547–562, 1998.

Ellison, T., Turbulent transport of heat and momentum from an infinite rough plane., *Journal of Fluid Mechanics*, *2*, 456–466, 1957.

Ellison, T., and J. Turner, Mixing of dense fluid in a turbulent pipe flow. Part 2: Dependence of transfer coefficients on local stability., *Journal of Fluid Mechanics*, *8*, 529–544, 1960.

Fleury, M., and R. Lueck, Direct heat flux estimates using a towed body., *Journal of Physical Oceanography*, *24*(4), 801–818, 1994.

Gargett, A., and J. Moum, Mixing efficiencies in turbulent tidal fronts: Results from direct and indirect measurements of density flux., *Journal of Physical Oceanography*, *25*(11 Pt I), 2583–2608, 1995.

Gargett, A., T. Osborn, and P. Nasmyth, Local isotropy and the decay of turbulence in a stratified fluid., *Journal of Fluid Mechanics*, *144*, 231–280, 1984.

Gibson, C., C. Friehe, and S. McConnell, Structure of sheared turbulent fluids., *Physics of Fluids*, *20*(Supplement), S156–S167, 1977.

Gill, A., *Atmosphere-Ocean Dynamics.*, 662 pp., Academic Press, 1982.

Gill, A., On the behaviour of internal waves in the wakes of storms., *Journal of Physical Oceanography*, *14*(7), 1129–1151, 1984.

Grant, H., R. Stewart, and A. Moilliet, Turbulence spectra from a tidal channel., *Fluid Mechanics*, *12*, 241–268, 1962.

Gregg, M., Diapycnal mixing in the thermocline: A review., *Journal of Geophysical Research*, *92*(C5), 5249–5286, 1987.

Gregg, M., E. D'Asaro, T. Shay, and N. Larson, Observations of persistent mixing and near-inertial internal waves., *Journal of Physical Oceanography*, *16*, 856–885, 1986.

Gurvich, A., and A. Yaglom, Breakdown of eddies and probability distributions for small-scale turbulence., *Physics of Fluids*, *10*(Supplement), S59–S65, 1967.

Hebert, D., J. Moum, C. Paulson, and C. Caldwell, The role of turbulent stress divergence in the equatorial Pacific zonal momentum balance., *Journal of Geophysical Research*, *96*(C4), 7127–7136, 1991.

Imberger, J., and G. Ivey, On the nature of turbulence in a stratified fluid. Part II: Application to lakes., *Journal of Physical Oceanography*, *21*(5), 659–680, 1991.

Itsweire, E., K. Helland, and C. van Atta, The evolution of grid-generated turbulence in a stably stratified fluid., *Journal of Fluid Mechanics*, *162*, 299–338, 1986.

Ivey, G., and J. Imberger, On the nature of turbulence in a stratified fluid. Part I: The energetics of mixing., *Journal of Physical Oceanography*, *21*(5), 650–658, 1991.

Kolmogorov, A., Local structure of turbulence in an incompressible fluid at very high Reynolds' number, *Doklady Akad. Nauk. SSSR*, *30*(4), 299–303, 1941*a*.

Kolmogorov, A., On the logarithmical normal particle size caused by particle crushing., *Doklady Akad. Nauk. SSSR*, *31*, 99–102, 1941*b*.

Large, W., and S. Pond, Open ocean momentum flux measurements in moderate to strong winds., *Journal of Physical Oceanography*, *11*(3), 324–336, 1981.

Leaman, K., and T. Sanford, Vertical energy propagation of inertial waves: A vector spectral analysis of velocity profiles., *Journal of Geophysical Research*, *80*(15), 1975–1978, 1975.

Lombardo, C., and M. Gregg, Similarity scaling of viscous and thermal dissipation in a convecting surface boundary layer., *Journal of Geophysical Research*, *94*(C5), 6273–6284, 1989.

Lueck, R., Microstructure measurements in a thermohaline staircase., *Deep-Sea Research*, *34*(10A), 1677–1688, 1987.

Lueck, R., D. Huang, D. Newman, and J. Box, Turbulence measurement with a moored instrument., *Journal of Atmospheric and Oceanic Technology*, *14*(1), 143–161, 1997.

Marmorino, G., L. Rosenblum, and C. Trump, Fine-scale temperature variability: The influence of near-inertial waves., *Journal of Geophysical Research*, *92*(C12), 13049–13062, 1987.

Miles, J., On the stability of heterogeneous shear flows., *Journal of Fluid Mechanics*, *10*, 496–508, 1961.

Moum, J., Efficiency of mixing in the main thermocline., *Journal of Geophysical Research*, *101*(C5), 12057–12096, 1996.

Moum, J., M. Gregg, R. Lien, and M. Carr, Comparison of turbulence kinetic energy dissipation rate estimates from two ocean microstructure profilers., *Journal of Atmospheric and Oceanic Technology*, *12*(2), 346–366, 1995.

Moum, J., and R. Lueck, Causes and implications of noise in oceanic dissipation measurements., *Deep-Sea Research*, *32*(4), 379–390, 1985.

Mudge, T., and R. Lueck, Digital signal processing to enhance oceanographic observations., *Journal of Atmospheric and Oceanic Technology*, *11*(3), 825–836, 1994.

Nasmyth, P., Oceanic turbulence., Ph.D. thesis, University of British Columbia, Canada, September, 1970.

Ninnis, R., The effects of spatial averaging on airfoil probe measurements of oceanic velocity microstructure., Ph.D. thesis, University of British Columbia, Canada, October, 1984.

Oakey, N., Determination of the rate of dissipation of turbulent energy from simultaneous temperature and velocity shear micro-structure measurements., *Journal of Physical Oceanography*, *12*(3), 256–271, 1982.

Osborn, T., Estimates of the local rate of vertical diffusion from dissipation measurements., *Journal of Physical Oceanography*, *10*(1), 83–89, 1980.

Osborn, T., and W. Crawford, An airfoil probe for measuring turbulent velocity fluctuations in water., in *Air-Sea Interaction Instruments and Methods.*, edited by F. Dobson, L. Hasse, and R. Davis, chapter 19, 369-386 pp., Plenum Press, New York, 1980.

Ozmidov, R., On the turbulent exchange in a stably stratified ocean., *Izv. Acad. USSR Atmos. Oceanic Phys.*, *1*(853-860), 1965, Engl. Transl.

Peters, H., M. Gregg, and J. Toole, On the parameterization of equatorial turbulence., *Journal of Geophysical Research*, *93*(C2), 1199–1218, 1988.

Pinkel, R., and C. Friehe, Summary reports: Marine boundary layer accelerated research initiative experiment review., *Tech. rep.*, , Scripps Institution of Oceanography, 1996.

Rines, J., J. Sullivan, P. Donaghay, and M. McFarland, Observations on the effects of wind-forced turbulence on the structural integrity of chain-forming diatoms., 1999, Submitted to American Society of Limnology and Oceanography, Ocean Sciences spring meeting, Santa Fe.

Rosenblum, L., and G. Marmorino, Statistics of mixing patches observed in the Sargasso Sea., *Journal of Geophysical Research*, *95*(C4), 5349–5357, 1990.

Screenivasan, K., and S. Tavoularis, Skewness of temperature derivatives in turbulent flows., *Physics of Fluids*, *20*, 1986–1988, 1980.

Shay, T., and M. Gregg, Convectively driven turbulent mixing in the upper ocean., *Journal of Physical Oceanography*, *16*(11), 1777–1798, 1986.

Sherman, F., J. Imberger, and G. Corcos, Turbulence and mixing in stratified waters., *Annual Review of Fluid Mechanics*, *10*, 267–288, 1978.

Sreenivasan, K., and R. Antonia, Skewness of temperature derivatives in turbulent shear flows., *Physics of Fluids*, *20*(12), 1986–1988, 1977.

Stacey, M., S. Monismith, and J. Burau, Observations of turbulence in a partially stratified estuary., 1997, Submitted to Journal of Physical Oceanography.

Stewart, R., The problem of diffusion in a stratified fluid., *Advances in Geophysics*, *6*, 303–311, 1959.

Stewart, R., Turbulence and waves in a stratified atmosphere., *Radio Science*, *4*(12), 1269–1278, 1969.

Stillinger, D., K. Helland, and C. van Atta, Experiments on the transition of homogeneous turbulence to internal waves in a stratified fluid., *Journal of Fluid Mechanics*, *131*, 91–122, 1983.

Tandon, A., and C. Garrett, Mixed layer re-stratification due to a horizontal density gradient., *Journal of Physical Oceanography*, *24*(6), 1419–1424, 1994.

Taylor, G., Internal waves and turbulence in a fluid of variable density., *Conseil Perm. Int. pour l'Expl. de la Mer., Rapp. et Proc-Verb*, *76*, 35–42, 1931.

Tennekes, H., and J. Lumley, *A First Course in Turbulence.*, 300 pp., MIT Press, 1972.

Thorpe, S., Experiments on instability and turbulence in a stratified shear flow., *Journal of Fluid Mechanics*, *61*(4), 731–751, 1973*a*.

Thorpe, S., Turbulence in stably stratified fluids: A review of laboratory experiments., *Boundary-Layer Meteorology*, *5*, 95–119, 1973*b*.

Thorpe, S., Turbulence and mixing in a Scottish loch., *Transactions of the Royal Society (London)*, *A286*, 125–181, 1977.

Thorpe, S., M. Curé, and M. White, The skewness of temperature derivatives in oceanic boundary layers., *Journal of Physical Oceanography*, *21*(3), 428–433, 1991.

Thorpe, S., and A. Hall, The mixing layer of Loch Ness., *Journal of Fluid Mechanics*, *101*, 687–703, 1980.

Toole, J., and R. Schmitt, Fine and micro-scale structures in the north-west Atlantic sub-tropical front., *Nature*, *327*, 47–49, 1987.

Townsend, A., Turbulent flow in a stably stratified atmosphere., *Journal of Fluid Mechanics*, *3*, 361–372, 1958.

van Atta, C., and T. Yeh, Evidence for scale similarity of internal intermittency in turbulent flows at large Reynolds numbers., *Journal of Fluid Mechanics*, *71*, 417–440, 1975.

Wolk, F., Near surface heat flux measurements with a towed vehicle., Master's thesis, University of Victoria, British Columbia, Canada, 1997.

Woods, J., and R. Wiley, Billow turbulence and ocean microstructure., *Deep-Sea Research*, *19*, 87–121, 1972.

Wyngaard, J., O. Coté, and Y. Izumi, Local free convection, similarity and the budgets of shear stress and heat flux., *Journal of the Atmospheric Sciences*, *28*, 1171–1182, 1971.

Yamazaki, H., and R. Lueck, Why oceanic dissipation rates are not log-normal., *Journal of Physical Oceanography*, *20*(12), 1907–1918, 1990.

Yamazaki, H., R. Lueck, and T. Osborn, A comparison of turbulence data from a submarine and a vertical profiler., *Journal of Physical Oceanography*, *20*(11), 1778–1786, 1990.

Appendix A

A reference of symbols and scales

Uppercase Roman letters

Symbol	*Quantity*	*Units*
B	buoyant production of kinetic energy	m^2s^{-3}
E_{10}	wind work at 10 m height	
	$\equiv \tau U_{10}$	Wm^{-2}
Fr_t	Turbulent Froude number	
	$\equiv (S^{3/2}/3N^{3/2})^{2/3} \approx 0.48 Ri_g^{-1/2}$	
H	depth of the ocean surface layer	m
J_b^0	surface buoyancy flux	
	$\equiv g/\rho(-\alpha J_q^0/c_p + \beta s J_q^e/L_e(1-s)$	WKg^{-1}
J_q^0	surface heat flux	
	$\equiv J_q^{sw} + J_q^{lw} + J_q^e + J_q^s$	Wm^{-2}
J_q^e	latent heat flux	Wm^{-2}
J_q^{lw}	longwave radiative flux	Wm^{-2}
J_q^s	sensible heat flux	Wm^{-2}
J_q^{sw}	shortwave radiative flux	Wm^{-2}

Symbol	*Quantity*	*Units*
K_H	eddy coefficient of heat	m^2s^{-1}
K_M	eddy coefficient of momentum	m^2s^{-1}
K_ρ	eddy coefficient of density	
	$\equiv \Gamma\epsilon/N^2$	m^2s^{-1}
$\mathcal{L}$	domain scale of turbulence	m
L	Monin-Obukov length	
	$\equiv u_*^3/\kappa J_b^0$	m
L_E	Ellison scale	
	$\equiv \overline{(\rho'^2)}^{1/2}\left(\frac{\partial\rho}{\partial z}\right)^{-1}$	m
L_e	Latent heat of evaporation	JKg^{-1}
L_K	Kolmolgorov scale	
	$\equiv (\nu^3/\epsilon)^{1/4}$	m
L_O	Ozmidov scale	
	$\equiv (\epsilon/N^3)^{1/2}$	m
N	Brunt-Väisälä frequency	s^{-1}
P	pressure	db
P_t	turbulent production of kinetic energy	m^2s^{-3}
P_*	reference pressure	db

Symbol	*Quantity*	*Units*
Ro	Rossby number	
	$\equiv U/f_c L$	m
Re_b	buoyancy Reynolds' number	
	$\equiv (L_O/L_K)^{4/3} = \epsilon/\nu N^2$	
Re_t	turbulent Reynolds' number	
	$\equiv 4.3\epsilon/\nu S^2$	
Rf	flux Richardson number	
	$\equiv B/P_t$	
Ri_g	gradient Richardson number	
	$\equiv N^2/S^2$	
S	10 m averaged shear	
$\mathtt{S_k}$	temperature gradient skewness	
T	temperature	^{o}C
T_t	turbulence time scale	
	$\equiv \gamma^{-1}$	s
T_τ	time scale	s
U_i	mean flow velocity	ms^{-1}

Lowercase Roman letters

Symbol	*Quantity*	*Units*
c_p	specific heat at constant pressure	$\mathrm{JKg^{-1}K^{-1}}$
f	frequency	$\mathrm{s^{-1}}$
f_c	Coriolis frequency	$\mathrm{s^{-1}}$
g	acceleration due to gravity	$\mathrm{ms^{-2}}$
k	wavenumber	cpm
l	length scale of turbulent overturns	m
p	pressure deviation from the mean	db
s	salinity	psu
sinc	sinc function $\equiv \sin x/x$	
t	time	s
u_i	turbulent velocity fluctuation	$\mathrm{ms^{-1}}$
u_*	friction velocity	$\mathrm{ms^{-1}}$
x_i	distance	m

Uppercase Greek letters

Symbol	*Quantity*	*Units*
Γ	mixing efficiency	
	$\equiv Rf/1 - Rf$	
Π	mean pressure	db

Lowercase Greek letters

α	coefficient of thermal expansion	$^{o}\mathrm{C}^{-1}$
β	coefficient of haline contraction	psu^{-1}
γ	adiabatic lapse rate	$\mathrm{K\ km}^{-1}$
γ_c	coherency	
γ_t	turbulent rate of strain	
	$\equiv (\epsilon/\nu)^{1/2}$	s^{-1}
ϵ	rate of viscous dissipation	
	$\equiv 7.5\nu\overline{(\partial w/\partial x)^2}$	WKg^{-1}
ϵ_f	buoyancy scaling for dissipation	
	$\equiv J_b^0$	WKg^{-1}
ϵ_s	wind stress scaling for dissipation	
	$\equiv u_*^3/\kappa z$	WKg^{-1}

Symbol	*Quantity*	*Units*
ϵ_{tr}	transition dissipation rate for wave-like motions	
	$\equiv 20\nu N^2$	WKg^{-1}
η	aspect ratio of Kelvin-Helmholtz billows	
κ	von Kármán's constant = 0.4	
λ	wavelength	m
μ	dynamic viscosity	$\mathrm{Kg\ m^{-1}s^{-1}}$
ν	kinematic viscosity	
	$\equiv \mu/\rho$	$\mathrm{m^2s^{-1}}$
ξ_i	breakage coefficient	
ρ	density	$\mathrm{Kg\ m^{-3}}$
ρ_0	reference density	
$\overline{\rho}$	mean density	
ρ'	density deviation from the mean	
τ	wind stress	pascals
ω	vorticity	$\mathrm{s^{-1}}$

Appendix B

The Ninnis correction for lost variance

The finite size of the shear probe used to measure the turbulent velocities means that the probe effectively acts as a low pass filter. The shear probe smooths high wavenumbers spatially and so high frequency velocity fluctuations are attenuated. As a result of this attenuation, the dissipation calculated by integrating the shear spectrum is an under-estimate. Oakey (1982) approximated the transfer function of the attenuation by a single pole filter:

$$H^2(k) = \frac{1}{1 + (k\lambda_c)^2} \tag{B.1}$$

where k is the wavenumber and λ_c is the cut-off wavelength. The cut-off wavelength is the highest detectable wavelength which is estimated as twice the length of the probe.

The problem with Oakey's correction is that the application of an approximated filter is rather unphysical and doesn't account for some low wavenumber behaviour. Ninnis (1984) compared the spectra measured in the laboratory by shear probes with spectra from high spatial resolution laser doppler anemometry and proposed a 3-dimensional model to explain the behaviour of the probes and derived a transfer

function which is independent of the rate of dissipation:

$$H^2(k) = 1 - 0.164\frac{k}{k_o} - 4.537\left(\frac{k}{k_o}\right)^2 + 5.503\left(\frac{k}{k_o}\right)^3 - 1.804\left(\frac{k}{k_o}\right)^4 \tag{B.2}$$

where k_o is the cut-off wavenumber. In the MBL experiment, two sizes of shear probe were deployed on *TOMI*: An experimental small probe with a cut-off wavenumber of 196 cpm and a well tested large probe with a cut-off wavenumber of 121 cpm. A comparison of the transfer functions for the Ninnis and Oakey corrections is given in figure B.1.

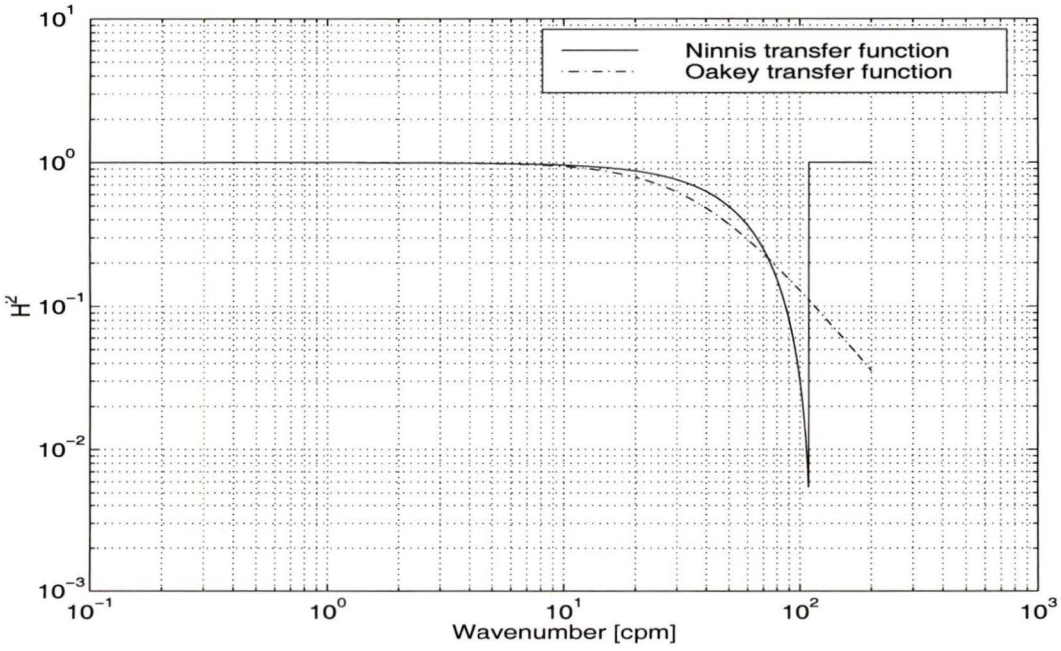

Figure B.1: Comparison of Oakey (1982) and Ninnis (1984) transfer functions. Cut-off wavelength, λ_c is 0.026 m ($k_o = 121$ cpm).

From this it can be seen that the Ninnis correction is smaller than the Oakey

correction between 9 and 70 cpm and larger from 70 cpm to the pole at 121 cpm. Figure B.2 compares the universal spectrum (Nasmyth 1970) with an uncorrected and a Ninnis corrected spectrum for 5 minutes of dissipation data from file mbl099 (JD116.243-116.262, tow 1).

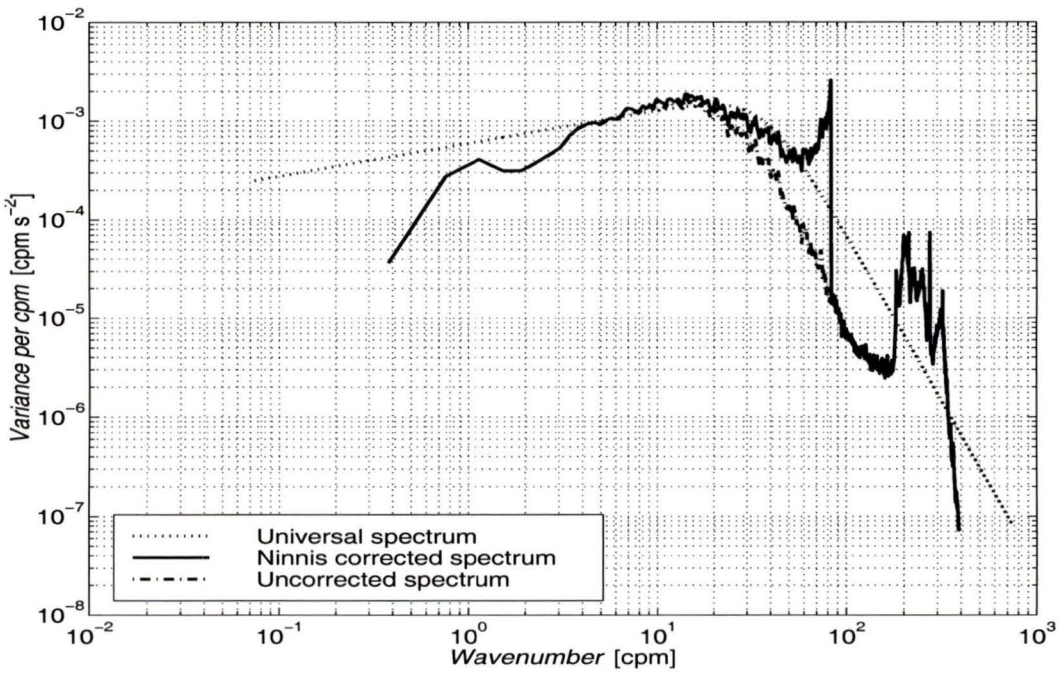

Figure B.2: Comparison universal spectrum with uncorrected and Ninnis corrected spectrum for a large probe measuring $\partial w/\partial x$ during tow 1. The corrected dissipation estimate of 5.37×10^{-7} W Kg^{-1} is 22% larger than the uncorrected spectrum. As above, λ_c is 0.026 m ($k_o = 121$ cpm).

Appendix C

Estimating the shear variance

As can be seen in figure B.2 the Ninnis correction has a pole and so it is important to avoid integrating into this region. Even without the correction there is a point at which noise is encountered. In order to avoid this high wavenumber noise contamination but ensure that the universal shear spectrum (Nasmyth 1970) was sufficiently resolved, an algorithm was used to check for deviation away from the universal form.

The method used here is essentially the same as that described in Moum *et al.* (1995). Integration of the spectrum is initially made between 1 and 20 cpm (well below half the Kolmogorov wavenumber) to give an estimated dissipation level, ϵ'. The universal spectrum which has a level equivalent to ϵ' is then calculated. This universal spectrum is integrated over the same waveband (1 - 20 cpm) to give ϵ_{univ}. Since ϵ' is much lower than the total variance of the measured spectrum, $\epsilon_{univ} < \epsilon'$, and so a new universal spectrum is calculated for a dissipation level of $\epsilon' + \epsilon_{univ}/\epsilon'$. This procedure is repeated and with each iteration, ϵ_{univ} converges with ϵ'. When the two spectra agree over the 1 - 20 cpm waveband to within 5%, the universal spectrum is integrated out to the Kolmogorov wavenumber and that is accepted as the final result. Figure B.2 shows that this iterative fitting procedure works very well.

Appendix D

Removal of coherent accelerations

As mentioned in section 5.2, body vibrations are a frequent source of contamination of the high frequency shear signal. The coherency, γ_c, of the accelerometer and high frequency shear was calculated, where γ_c is defined by:

$$\gamma_c^2(f) = \frac{< |C_{xy}(f)|^2 >}{C_{xx}(f)C_{yy}(f)} \tag{D.1}$$

C_{xy} is the cross-spectrum of x, y and C_{xx}, C_{yy} are the auto-spectra. The z accelerometer was used to remove coherent motions from the w probes and the y accelerometer was used to calculate coherency with the v probes. The shear spectrum was then multiplied by $1 - \gamma_c^2$ to remove coherent accelerations. In both strong and weak turbulence, the coherency was generally low. The mean coherency in figure D.1 is 0.06 and is only significant in the low frequencies (below 10 Hz) and high frequency noise. In weak turbulence, even this high frequency coherency is lost. The coherency reduces the shear signal by 19% in comparison with the uncorrected spectrum over the waveband 0.15-20 Hz in the example shown here. The Ninnis correction increases the shear signal by 20% over the waveband 20-70 Hz. Hence these two corrections are similar in magnitude but opposite in sign during this tow.

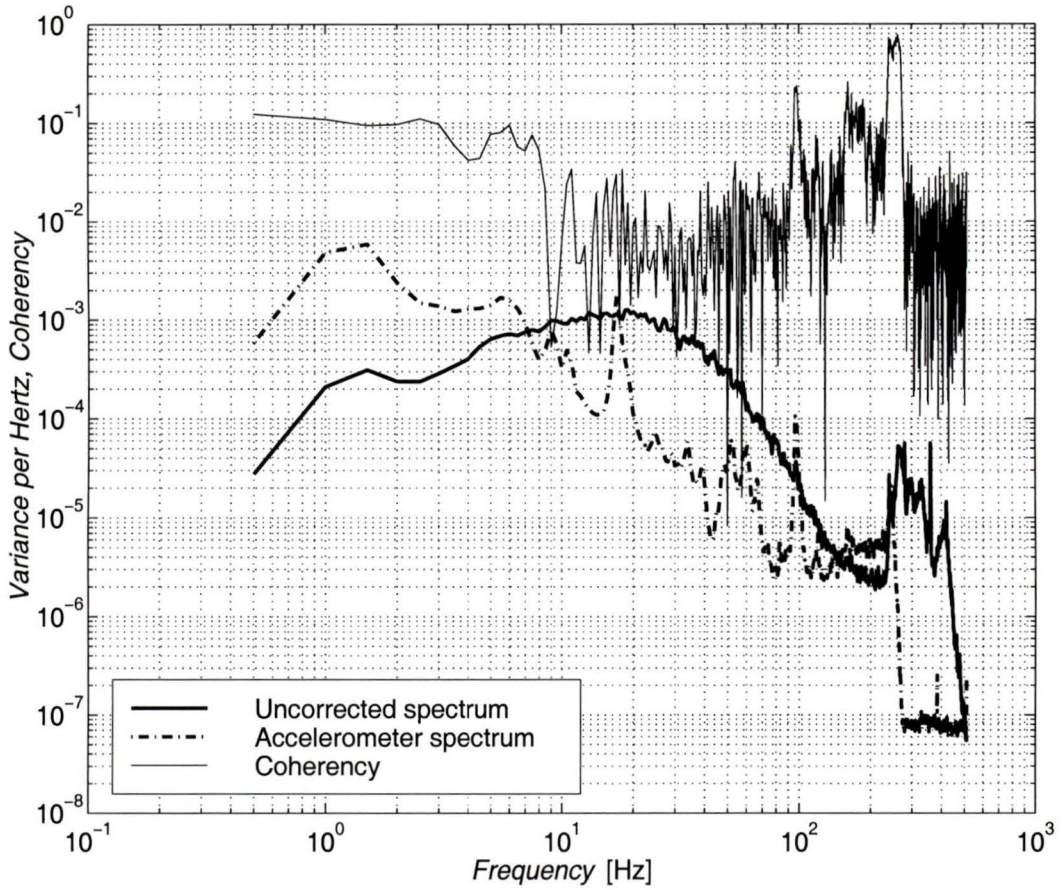

Figure D.1: Shear and accelerometer spectra from tow 1 and the coherency of the two signals (file mbl099, 0-300 s).

VITA

Surname: HOLGATE Given Names: Simon John

Place of Birth: Pembury, Kent, England

Educational Institutions Attended:

University of Victoria	1995 to 1998
University of Liverpool	1992 to 1995
Mid-Kent College of Higher and Further Education	1989 to 1992

Degrees Awarded:

B.Sc. (Honours) 1st Class	University of Liverpool	1995

Honours and Awards:

Muriel Owen Mature Students' Scholarship	1993, 1994, 1995
Roxby Memorial Prize	1994,1995
Humboldt Prize in Geography	1995
Hamilton Oil Co. "Eco-Education Award" - runner up	1994
Wilfred Smith Prize	1993

Publications:

None

Partial Copyright License

I hereby grant the right to lend my thesis to users of the University of Victoria Library, and to make single copies only for such users or in response to a request from the Library of any other university, or similar institution, on its behalf or for one of its users. I further agree that permission for extensive copying of this thesis for scholarly purposes may be granted by me or a member of the University designated by me. It is understood that copying or publication of this thesis for financial gain shall not be allowed without my written permission.

Title of Thesis:

Low Richardson Number Turbulence in the Ocean Surface Layer.

Author: [redacted]

Simon Holgate

November 12, 1998